IMPROVED STOCHASTIC ESTIMATORS FOR DISCONNECTED CONTRIBUTIONS TO MESONIC FORM FACTORS IN LATTICE QCD

DIPLOMARBEIT IM FACHBEREICH PHYSIK

VERA MAGDALENA GÜLPERS

Institut für Kernphysik
Johannes Gutenberg-Universität Mainz

25. Mai 2011

ABSTRACT

To determine certain physical quantities like form factors, diagrams containing quark disconnected loops have to be considered. For the calculation of these loops one needs the quark propagator which on a space-time lattice requires the inversion of a very large matrix. Since an explicit calculation is too expensive in computer time, such inversions have to be done stochastically. In this thesis some methods to improve the stochastic estimates for the disconnected loops are tested. It is figured out which method works best, and the required parameters are tuned to obtain an optimal balance between the remaining statistical errors and the required computer time. Finally, the disconnected contribution to the scalar form factor of the pion at zero momentum transfer $Q^2 = 0$ is calculated.

ZUSAMMENFASSUNG

Bei der Berechnung bestimmter physikalischer Größen wie Formfaktoren erhält man Beiträge von Diagrammen mit unverbundenen Quarkschleifen. Um solche Schleifen zu berechnen, benötigt man den Quarkpropagator. Diesen erhält man auf einem Raum-Zeit Gitter durch Invertieren einer sehr großen Matrix. Da eine explizite Rechnung zu viel Rechenzeit erfordert würde, müssen solche Matrizen stochastisch invertiert werden. In der vorliegenden Arbeit werden einige Methoden zur Verbeserung des stochastischen Schätzers für die unverbundenen Schleifen getestet. Die beste Methode wird bestimmt und die benötigten Parameter so angepasst, dass eine optimale Balance zwischen dem verbleibenden statistischen Fehler und der erforderlichen Rechenzeit entsteht. Zuletzt wird der unverbundene Beitrag zum skalaren Formfaktor des Pions bei verschwindendem Impulsübertrag $Q^2 = 0$ berechnet.

CONTENTS

INTRODUCTION

The Standard Model of particle physics [1] is the established theory to describe the fundamental particles and their interactions. The interactions contained in the Standard Model are the electromagnetic, the weak and the strong force, where the electromagnetic and the weak force can be unified to the so-called electroweak interaction. While the strong force only acts on the quarks, the electroweak force couples to both quarks and leptons. The three fundamental interactions can be described by gauge theories, where the gauge bosons are the carriers of the force. The gauge theory that corresponds to the strong force is called Quantum Chromodynamics (QCD) [2]. A more detailed introduction to QCD will be given in chapter 1. The associated gauge bosons, i.e. the mediators of the strong force, are the gluons. Gluons couple to objects that carry colour, which is the charge that belongs to the strong interaction. Three different colours are possible, conventionally called red, green and blue. Every quark has a colour, thus quarks can interact with each other via the strong force. Since gluons carry colour, self interactions between gluons are also possible. The strength of the coupling of the strong interaction depends on the energy region where the interaction takes place. The running coupling has two interesting features. For high energies the coupling becomes small, thus the quarks and gluons become asymptotically free. For small energies the coupling becomes strong and quarks and gluons are confined to bound states called hadrons. While in the region of small coupling perturbative expansions in the coupling constant can be performed, such an expansion is not possible in the low energy region. In 1974, K. Wilson developed a method to treat QCD non-perturbatively by introducing an Euclidean space-time lattice [3]. Through the discretisation of the space-time QCD is regularised. Due to the finite lattice spacing one obtains a natural momentum cutoff, thus the ultraviolet divergences appearing in loop integrals are removed. Another advantage of introducing a space-time lattice is that numerical techniques from statistical mechanics can be used and numerical simulations of physical processes on computers are possible. A short introduction to lattice QCD can be found in chapter 2.

Many physical quantities that can be calculated in lattice QCD contain contributions from diagrams with disconnected quark lines. In the following these diagrams are called disconnected diagrams, where the terminology "disconnected" refers to quark disconnected and does not exclude gluons connecting two quark lines. In the following we will concentrate on diagrams with a disconnected loop, thus a disconnected quark line from one lattice point to the same point. Quantities containing disconnected loops are for example the scalar form factor of the pion [4] or the strangeness content of the nucleon [5]. In the following we will concentrate on the scalar form factor of the pion. A short introduction to pions and form factors will be given in sections 1.3 and 1.4. The scalar form factor describes the coupling of a scalar particle to a pion, for example the coupling of a Higgs boson to a pion [6]. Since the Higgs boson

has so far not been discovered, no experimental value for the scalar form factor of the pion exists. Thus one has to obtain values from theoretical calculations. However, lattice QCD provides a reasonable possibility to calculate form factors. While for the vector form factor, which occurs in the coupling of a photon to a pion, one can show [7] that the disconnected contribution vanishes, one expects the disconnected contribution to the scalar form factor to be non-zero. Thus it is important to develop methods to calculate these contribution as accurately as possible. However, the calculation of diagrams containing disconnected loops requires more numerical effort than the calculation of connected parts, since the propagator from every lattice point to all lattice points – the so-called all-to-all propagator – is needed. On the lattice this requires an inversion of a $12V \times 12V$ matrix, where V is the total number of lattice points and 12 results from three colour- and four Dirac-components. Since V is usually of $\mathcal{O}(10^6)$ and higher, an exact calculation using point sources (see section 3.1) is too expensive in computer time. Therefore the matrix has to be inverted stochastically. This is done using the method of stochastic sources [8], which is introduced in section 3.2. To invert the matrix, one has to solve the Dirac equation on the lattice for every stochastic source. Since the solution of the Dirac equation is expensive in computer time, one is interested in using as few sources as possible. However, fewer sources result in larger statistical errors, which requires the development of techniques to improve the stochastic estimates. Three techniques [9] – dilution, the hopping parameter expansion, and the truncated solver method – will be introduced in sections 3.3 to 3.5. In chapter 4 all three methods will be tested with the Klein-Gordon operator as a toy model on a two-dimensional 10×10 lattice. The tests will then be continued using the Wilson-Dirac operator in chapter 5. At first the loop will be calculated for the unimproved Wilson-Dirac operator on an 8×8^3 lattice and afterwards for the $\mathcal{O}(a)$-improved Wilson-Dirac operator using four different lattices. Here the hopping parameter expansion has to be adapted to the case of the improved Wilson-Dirac operator. It will be figured out which method works most efficiently and the required parameters will be tuned for one of the tested lattices such that one obtains an optimal balance between the remaining statistical error and the computer time needed for the calculation.
In chapter 6 we will discuss how the disconnected contribution to the scalar form factor can be extracted from lattice calculations using the so-called summation method [10]. Finally the disconnected contribution to the scalar charge, thus the scalar form factor for zero momentum transfer $Q^2 = 0$, will be calculated for the E4 ensemble, where the parameters for the calculation of the loop have already been tuned.

1

THEORETICAL BACKGROUND

1.1 QCD AS A GAUGE THEORY

Quantum Chromodynamics (QCD) is a non-Abelian gauge theory in $SU(3)$ colour-space. Since $SU(3)$ has eight generators, there exist eight gluons which mediate the strong force. The Lagrangian density of QCD is given by [2]

$$\mathcal{L} = \overline{\Psi}(i\gamma_\mu D^\mu - m)\Psi + \frac{1}{2g^2}\mathrm{Tr}\left[\left(F^a_{\mu\nu}t^a\right)^2\right], \tag{1.1}$$

where the t^a with $a = 1, \ldots, 8$ are the eight generators of $SU(3)$, which can be represented by the Gell-Mann matrices. D_μ is the covariant derivative

$$D_\mu = \partial_\mu + iA^a_\mu t^a \tag{1.2}$$

with the gauge fields A^a_μ and the strong coupling g. The field strength tensor $F^a_{\mu\nu}$ for the strong interaction is given by

$$F^a_{\mu\nu} = \partial_\mu A^a_\nu - \partial_\nu A^a_\mu - f^{abc}A^b_\mu A^c_\nu\,. \tag{1.3}$$

The f^{abc} are the $SU(3)$ structure constants. They are defined by the commutators of the generators of the group

$$\left[t^a, t^b\right] = if^{abc}t^c\,. \tag{1.4}$$

The Lagrangian (1.1) is invariant under local $SU(3)$ gauge transformations

$$\begin{aligned}
\Psi(x) &\to \Psi'(x) = \Omega(x)\Psi(x)\\
\overline{\Psi}(x) &\to \overline{\Psi}'(x) = \overline{\Psi}(x)\Omega(x)^\dagger\\
A^a_\mu(x)t^a &\to A'^a_\mu(x)t^a = \Omega(x)A^a_\mu(x)t^a\Omega(x)^\dagger + i\left(\partial_\mu\Omega(x)\right)\Omega(x)^\dagger
\end{aligned} \tag{1.5}$$

with a local $SU(3)$ matrix $\Omega(x)$.

1.2 THE RUNNING COUPLING CONSTANT

In QCD one can define an analogue of the fine structure constant

$$\alpha_s = \frac{g^2}{4\pi}\,. \tag{1.6}$$

As in QED, α_s is not a constant but depends on the momentum transfer Q^2. Such a Q^2 dependence of the coupling constant is known as running coupling. After renormalisation of QCD at a scale Λ one finds as a solution of the renormalisation group equation [2]

$$\alpha_s(Q^2) = \frac{\alpha_s(\Lambda^2)}{1 + \alpha_s(\Lambda^2)\frac{33-2n_f}{12\pi}\log(\frac{Q^2}{\Lambda^2})} \tag{1.7}$$

with the number $n_f = 6$ of quark flavours in the standard model. For large momentum transfers, i.e. small distances, the coupling α_s becomes small, which leads to the so called asymptotic freedom.
For small momentum transfers, i.e. large distances, the strong interaction gets strong. This behaviour indicates confinement, which means that quarks or gluons cannot exist as free particles. In this region perturbation theory cannot be used anymore. However, QCD can be regularised by introducing a space-time lattice. With lattice QCD one has the possibility to study also non-perturbative phenomena.

1.3 PIONS

Pions are pseudoscalar mesons consisting of a quark and an antiquark of the first generation. They have the quantum numbers $J^{PC} = 0^{-+}$. Three types of pions with different charges are possible

$$\pi^+ = |u\bar{d}\rangle \qquad \pi^- = |d\bar{u}\rangle \qquad \pi^0 = \frac{1}{\sqrt{2}}\left(|u\bar{u}\rangle - |d\bar{d}\rangle\right), \tag{1.8}$$

which form an isospin triplet. The masses [11] of the pions are

$$\begin{aligned} \pi^\pm &: \quad m = 139.57018 \pm 0.00035\,\text{MeV} \\ \pi^0 &: \quad m = 134.9766 \pm 0.0006\,\text{MeV}\,. \end{aligned} \tag{1.9}$$

Pions can be identified as pseudo-Goldstone bosons of the breaking of chiral symmetry. In exact chiral symmetry, thus vanishing masses for the light quarks, the Lagrangian for these quarks can be separated into a left- and a right-handed part.

$$\mathcal{L} = \overline{\Psi}_L i\gamma_\mu D^\mu \Psi_L + \overline{\Psi}_R i\gamma_\mu D^\mu \Psi_R \tag{1.10}$$

If n_f is the number of light flavours, both parts can be transformed separately by a global $SU(n_f)$ transformation in flavour-space

$$\Psi_{L/R} \to e^{i\alpha_i \gamma_5 t_i}\Psi_{L/R} \qquad \overline{\Psi}_{L/R} \to \overline{\Psi}_{L/R} e^{i\alpha_i \gamma_5 t_i} \tag{1.11}$$

with the generators t_i, $i = 1, \ldots, n_f^2 - 1$ of $SU(n_f)$. Thus the Lagrangian (1.10) has a global $SU(n_f)_L \times SU(n_f)_R$ symmetry. However, the QCD vacuum is not invariant under the full symmetry group $SU(n_f)_L \times SU(n_f)_R$, due to the non-vanishing quark condensate [2]

$$\langle 0|\overline{q}q|0\rangle = \langle 0|\overline{q}_L q_R + \overline{q}_R q_L|0\rangle \neq 0 \tag{1.12}$$

that mixes the two heliticities. The vacuum (1.12) is invariant only if right- and left-handed fields are transformed using the same $SU(n_f)$ matrix. Therefore the $SU(n_f)_L \times SU(n_f)_R$ symmetry is broken spontaneously to $SU(n_f)$. Due to the Goldstone theorem [12] $n_f^2 - 1$ massless Goldstone bosons occur.
Since the light quarks are not massless the $SU(n_f)_L \times SU(n_f)_R$ symmetry is also broken explicitly by the mass term in the Lagrangian. This mechanism generates masses for the (pseudo-) Goldstone bosons. If one only considers the two lightest flavours u and d, so $n_f = 2$, the associated pseudo-Goldstone bosons are the 3 pions ($\pi^\pm$,π^0). For $n_f = 3$ additionally the kaons and the η occur.

1.4 FORM FACTORS

Form factors $F(Q^2)$ contain information about the substructure of a particle. They describe how the differential cross section differs from the cross section of a point-like particle [13]

$$\frac{d\sigma}{d\Omega} = \left(\frac{d\sigma}{d\Omega}\right)_{\text{point}} \left|F(Q^2)\right|^2 \tag{1.13}$$

with the momentum transfer $q^2 = (p - p')^2$ and $Q^2 = -q^2$, where p is the four-momentum of the incoming and p' of the outgoing state. Form factors are measured in scattering experiments.
In the non-relativistic case, form factors can be written as the Fourier transform of the charge distribution. Therefore, in spherical symmetry, the form factor is related to the charge radius.

$$F(Q^2) = 1 - \frac{1}{6}\left\langle r^2\right\rangle Q^2 + \mathcal{O}(Q^4) \tag{1.14}$$

$$\left\langle r^2\right\rangle = -6\frac{dF(Q^2)}{dQ^2}\Big|_{Q^2=0} \tag{1.15}$$

For the charged pion for example the vector form factor can be calculated from the matrix element [4, 14, 15, 16, 17]

$$\langle \pi\left(p'\right)|V_\mu|\pi\left(p\right)\rangle = (p + p')_\mu F_V\left(Q^2\right) \tag{1.16}$$

with

$$V_\mu = \frac{2}{3}\bar{u}\gamma_\mu u - \frac{1}{3}\bar{d}\gamma_\mu d\,. \tag{1.17}$$

The vector form factor occurs in the coupling of a photon to a pion, for example in pion electron scattering.

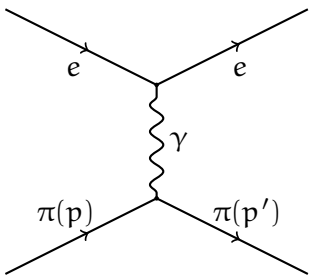

Figure 1.1: Feynman diagram of pion electron scattering

The scalar form factor can be calculated as [4, 14, 15, 18]

$$\langle \pi\left(p'\right)|S|\pi\left(p\right)\rangle = F_s\left(Q^2\right) \quad \text{with} \quad S = m_d\bar{d}d + m_u\bar{u}u\,. \tag{1.18}$$

This describes the coupling of a pion to a scalar particle such as the Higgs boson. Since the Higgs boson so far is not discovered, the only possibility to obtain values for the scalar form factor of the pions are theoretical calculations. Such calculations can be performed on space-time lattices.

2

QUANTUM FIELD THEORIES ON THE LATTICE

As mentioned above, QCD can be regularised by introducing a $T \times L^3$ lattice Λ in space-time

$$\Lambda = \left\{ n \in \mathbb{N}^4 \,|\, n_1, n_2, n_3 = 0, 1, ..., L-1 \,;\, n_0 = 0, 1, ..., T-1 \right\} \tag{2.1}$$

with T lattice points in time direction and L lattice points for each three spatial directions.

The lattice in momentum space is obtained by Fourier transformation. The dual lattice then is given by [19]

$$\Lambda^* = \left\{ p \in \mathbb{R}^4 \middle| p_0 = \frac{2\pi}{T} n_0 \,;\, p_i = \frac{2\pi}{L} n_i \right\} . \tag{2.2}$$

Here one can see that on the lattice the momenta are discrete and only values in the first Brillouin zone are allowed:

$$-\frac{\pi}{a} < p_\mu \leqslant \frac{\pi}{a} . \tag{2.3}$$

Therefore on the lattice one has a "natural" momentum cutoff.

The lattice Λ (2.1) is defined in Euclidean metric. To obtain Euclidean metric one has to switch to imaginary times $t \to i\tau$, a procedure called Wick rotation. In Euclidean metric the QCD action is given by [19]

$$S_E = \sum_{f=1}^{N_f} \int d^4x \overline{\Psi}^{(f)}(x) \left(\gamma_\mu D_\mu + m_f \right) \Psi^{(f)}(x) + \frac{1}{2g^2} \int d^4x \mathrm{Tr} \left[F_{\mu\nu}(x) F_{\mu\nu}(x) \right] \tag{2.4}$$

with the covariant derivative

$$D_\mu = \partial_\mu + iA_\mu \tag{2.5}$$

and the field strength tensor for the strong interaction

$$F_{\mu\nu} = \partial_\mu A_\nu - \partial_\nu A_\mu + i[A_\mu, A_\nu] . \tag{2.6}$$

Here we use the abbreviation $A_\nu^a t^a = A_\nu$.

The Euclidean gamma matrices have to fulfil the property

$$\{\gamma_\mu, \gamma_\nu\} = 2\delta_{\mu\nu} . \tag{2.7}$$

In the chiral representation they are given by [19]

$$\gamma_\mu = \begin{pmatrix} 0 & e_\mu \\ (e_\mu)^\dagger & 0 \end{pmatrix} \tag{2.8}$$

with $\quad e_0 = \mathbb{1}_{2\times 2} \quad$ and $\quad e_k = -i\sigma_k$.

In the following some quantum field theories we will use in chapters 4 and 5, namely the free Klein-Gordon theory, the free Dirac theory and QCD, will be formulated on the lattice.

2.1 THE KLEIN-GORDON OPERATOR ON THE LATTICE

First of all we will discretise the free Klein-Gordon operator D_{KG} on the lattice. Spin-0 particles with mass m fulfil the Klein-Gordon equation

$$\left(-\partial_\mu\partial_\mu + m^2\right)\Phi(x) = D_{KG}\Phi(x) = 0, \tag{2.9}$$

where the Euclidean metric is used. On the lattice the partial derivative in the Klein-Gordon operator is discretised using the difference quotient

$$\partial_\mu\partial_\mu\Phi(n) \to -\frac{2d}{a^2}\cdot\Phi(n) + \sum_{\mu=1}^{d}\frac{1}{a^2}\left(\Phi(n+a\mu)+\Phi(n-a\mu)\right), \tag{2.10}$$

where n are the coordinates in lattice units, $n + a\mu$ are the coordinates of the neighbouring point in μ direction, a is the lattice spacing and d the dimensionality.
In total the Klein-Gordon operator on the lattice can be written as

$$\boxed{D_{KG}\Phi(n) = \frac{m^2a^2+2d}{a^2}\Phi(n) - \sum_{\mu=0}^{d}\frac{1}{a^2}\left(\Phi(n+a\mu)+\Phi(n-a\mu)\right).} \tag{2.11}$$

D_{KG} can be seen as an $N\times N$ matrix where N is the total number of lattice points. The matrix D_{KG} can be separated into two parts, a part which is proportional to the unit matrix and a part H that only couples nearest neighbours. Therefore D_{KG} can be written as

$$D_{KG} = C\left(\mathbb{1} - \kappa H\right), \tag{2.12}$$

where for the Klein-Gordon operator κ is defined as

$$\kappa \equiv \frac{a^2}{2\left(m^2a^2+2d\right)} \tag{2.13}$$

and $C = 1/(2\kappa)$. Since applying H means "hopping" from one lattice point to a neighbouring point, H is called hopping matrix and κ the hopping parameter.

2.2 NAIVE DISCRETISATION OF THE DIRAC OPERATOR

In the following the Euclidean QCD action (2.4) will be discretised as described in [19][1].

As a starting point for the discretisation of QCD we look at the (Euclidean) action S_F^0 of a free fermion. In the continuum it is given by

$$S_F^0 = \int d^4x\,\overline{\Psi}(x)\left(\gamma_\mu\partial_\mu + m\right)\Psi(x). \tag{2.14}$$

When introducing the 4D lattice (2.1) with lattice spacing a the integral in (2.14) has to be replaced by a sum over all lattice points and the derivative by a

1 similar derivations can also be found for example in [20, 21, 22, 23]

symmetric difference quotient. Thus we obtain the discretisation of the free fermion action

$$S_F^0 = a^4 \sum_{n\in\Lambda} \overline{\Psi}(n) \left(\sum_{\mu=0}^{3} \gamma_\mu \frac{\Psi(n+a\mu) - \Psi(n-a\mu)}{2a} + m\Psi(n) \right) . \tag{2.15}$$

2.3 QCD ON THE LATTICE

As in the continuum, invariance under local $SU(3)$ transformations

$$\Psi(n) \to \Psi'(n) = \Omega(n)\Psi(n) \qquad \overline{\Psi}(n) \to \overline{\Psi}'(n) = \overline{\Psi}(n)\Omega(n)^\dagger \tag{2.16}$$

is required. Obviously the first summand of (2.15) is not gauge invariant. To construct a gauge invariant action one needs objects transforming like [19, 23]

$$U_\mu(n) \to U'_\mu(n) = \Omega(n)U_\mu(n)\Omega(n+a\mu)^\dagger . \tag{2.17}$$

Objects that have the required transformation behaviour are the so-called parallel transporters

$$U(x,y) = \text{P.O.}exp\left(-\int_y^x dz\, A_\mu(z) \right) , \tag{2.18}$$

where "P.O." stands for path ordering. Under $SU(3)$ gauge transformations (1.5) the $U(x,y)$ transforms as

$$U(x,y) \to \Omega(x)U(x,y)\Omega(y)^\dagger . \tag{2.19}$$

A parallel transporter between two neighbouring points n and $n+a\mu$

$$U(n,n+a\mu) = U_\mu(n) \to U'_\mu(n) = \Omega(n)U_\mu(n)\Omega(n+a\mu)^\dagger \tag{2.20}$$

is exactly what we need. The gauge fields $U_\mu(n)$ are elements of the gauge group $SU(3)$. They "live" on the links between two lattice points and therefore are called link variables. Some link variables are shown in figure 2.1.

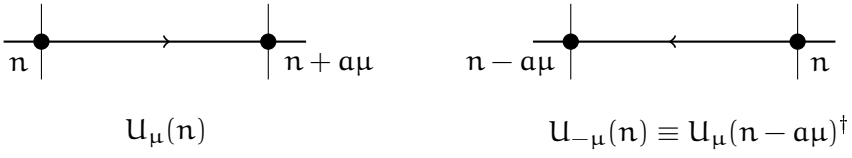

Figure 2.1: Link variables

Now a gauge invariant action can be constructed.

$$S_F = a^4 \sum_{n\in\Lambda} \overline{\Psi}(n) \left(\sum_{\mu=0}^{3} \gamma_\mu \frac{U_\mu(n)\Psi(n+a\mu) - U_{-\mu}(n)\Psi(n-a\mu)}{2a} + m\Psi(n) \right) \tag{2.21}$$

The smallest closed loop on the lattice, a so-called plaquette $U_{\mu\nu}(n)$, can be constructed as a product of four link variables,

$$U_{\mu\nu}(n) = U_\mu(n)U_\nu(n+a\mu)U_\mu(n+a\nu)^\dagger U_\nu(n)^\dagger \,. \tag{2.22}$$

A picture of a plaquette is shown in figure 2.2.

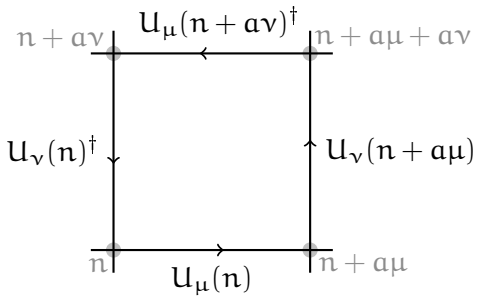

Figure 2.2: Plaquette $U_{\mu\nu}(n)$

Under the gauge transformation (2.17) the plaquette transforms as

$$U_{\mu\nu}(n) = \Omega(n)U_{\mu\nu}(n)\Omega(n)^\dagger \,. \tag{2.23}$$

Therefore the trace of a plaquette is gauge invariant. These traces can be used to construct the Wilson gauge action

$$S_G[U] = \frac{2}{g^2}\sum_{n\in\Lambda}\sum_{\mu<\nu}\mathrm{Re}\ \mathrm{Tr}\left[\mathbb{1} - U_{\mu\nu}(n)\right] \,. \tag{2.24}$$

2.4 FERMION DOUBLING AND WILSON-DIRAC OPERATOR

Rewriting the fermion action (2.21) as

$$S_F = a^4 \sum_{n,m\in\Lambda}\overline{\Psi}(n)D(n|m)\Psi(m) \tag{2.25}$$

results in the naive Dirac operator on the lattice

$$D(n|m) = \sum_{\mu=0}^{3}\gamma_\mu\frac{U_\mu(n)\delta_{n+a\mu,m} - U_{-\mu}(n)\delta_{n-a\mu,m}}{2a} + m\delta_{n,m} \,. \tag{2.26}$$

To calculate the Dirac operator in momentum space, $D(n|m)$ has to be Fourier transformed according to

$$\tilde{D}(p|q) = \frac{1}{|\Lambda|}\sum_{n,m\in\Lambda} e^{-ip\cdot na}\, D(n|m)\, e^{iq\cdot ma} \tag{2.27}$$

where $|\Lambda|$ is the total number of lattice points. Inserting (2.26) into the Fourier transformation one obtains

$$\tilde{D}(p|q) = \delta(p-q)\underbrace{\left(m\mathbb{1} + \frac{i}{a}\sum_{\mu=0}^{3}\gamma_\mu \sin(p_\mu a)\right)}_{\tilde{D}(p)} \,. \tag{2.28}$$

In addition to $p = (0,0,0,0)$, the massless Dirac operator in momentum space $\tilde{D}(p)|_{m=0}$ also vanishes if the components of the four momentum are either 0 or π/a. This leads to 16 poles representing 16 fermions on the lattice compared to one pole in the continuum. This problem is known as the so-called fermion doubling. It can be solved by adding an additional term to the Dirac operator in momentum space.

$$\tilde{D}(p) = m\mathbb{1} + \frac{i}{a}\sum_{\mu=0}^{3}\gamma_\mu \sin(p_\mu a) + \mathbb{1}\frac{1}{a}\sum_{\mu=0}^{3}(1-\cos(p_\mu a)) \tag{2.29}$$

Obviously the new summand in (2.29) only vanishes for the physical pole $p = (0,0,0,0)$. Transforming back to postition space one obtains an additional term in the Dirac operator

$$-\frac{a}{2}\sum_{\mu=0}^{3}\frac{\delta_{n+a\mu,m} - 2\delta_{n,m} + \delta_{n-a\mu,m}}{a^2}, \tag{2.30}$$

which has the form of a discretised second derivative. This term can also be made gauge invariant using gauge fields as done for the naive discretisation of the Dirac operator. In total the so-called Wilson-Dirac operator can be written as

$$\begin{aligned} D_W(n|m) &= \left(\frac{4}{a} + m\right)\delta_{m,n} \\ &- \frac{1}{2a}\sum_{\mu=0}^{3}\left(U_\mu(n)(1-\gamma_\mu)\delta_{n+a\mu,m} + U_{-\mu}(n)(1+\gamma_\mu)\delta_{n-a\mu,m}\right). \end{aligned} \tag{2.31}$$

Like the Klein-Gordon operator (2.11) the Wilson-Dirac operator consists of two parts. One part is proportional to the unit matrix $\mathbb{1}$ and the other part couples neighbouring points. Therefore it can be rewritten as

$$D_W = C\,(\mathbb{1} - \kappa H) \tag{2.32}$$

with the hopping parameter

$$\kappa = \frac{1}{2\,(am+4)} \qquad \text{and} \qquad C = m + 4/a\,. \tag{2.33}$$

In total the Wilson action is given by

$$\begin{aligned} S_W = a^4 \sum_{n\in\Lambda}\overline{\Psi}(n)\Bigg[&\left(m + \frac{4}{a}\right)\Psi(n) \\ &- \sum_{\mu=0}^{3}\frac{(\mathbb{1}-\gamma_\mu)U_\mu(n)\Psi(n+a\mu) + (\mathbb{1}+\gamma_\mu)U_{-\mu}(n)\Psi(n-a\mu)}{2a}\Bigg]. \end{aligned} \tag{2.34}$$

The additional Wilson term explicitly breaks the chiral symmetry even for massless quarks, thus (2.34) is not invariant under

$$\Psi(x) \to e^{i\alpha\gamma_5}\Psi(x) \qquad \overline{\Psi}(x) \to \overline{\Psi}(x)e^{i\alpha\gamma_5} \tag{2.35}$$

for $m = 0$ due to the non-vanishing anticommutator of the massless Wilson-Dirac operator $D_W|_{m=0}$ and γ_5 [19]

$$\gamma_5 \cdot D_W|_{m=0} + D_W|_{m=0} \cdot \gamma_5 \neq 0\,. \tag{2.36}$$

The No-Go Theorem

In an ideal theory the massless Dirac operator D on the lattice should fulfil the following properties [23]:

- D is local
- D has the right continuum limit $a \to 0$
- The theory is free of doublers
- Chiral symmetry is preserved, thus $\gamma_5 D + D\gamma_5 = 0$

In their no-go theorem [24] Nielsen and Ninomiya have shown that these four properties cannot be fulfilled simultaneously.

In lattice QCD several formulations of a discretised Dirac operator have been developed. However, due to the no-go theorem, in each formulation at least one of the four properties shown above has to be violated. Some common examples for discretised Dirac actions in lattice QCD are

WILSON-DIRAC (2.34): As we have already seen, the Wilson-Dirac operator breaks the chiral symmetry.

STAGGERED FERMION ACTION [25]: With staggered fermions the doublers are reduced to 4, while simultaneously a subgroup of chiral symmetry is preserved.

GINSPARG-WILSON [26]: The Ginsparg-Wilson action completely removes the doublers. It does not fulfil the property $\gamma_5 D + D\gamma_5 = 0$ but $\gamma_5 D + D\gamma_5 = aD\gamma_5 D$, which is a modified formulation of chiral symmetry on the lattice.

In the following we will concentrate on the Wilson-Dirac operator, which we will use for our calculations in chapters 5 and 6.

2.5 THE $\mathcal{O}(a)$-IMPROVED WILSON-DIRAC OPERATOR

The Wilson action (2.34) can be further improved following the guidelines of the so-called Symanzik improvement programme [27]. Here additional terms that vanish in the continuum limit $a \to 0$ can be added to the action

$$S_{\text{eff}} = a^4 \sum_{n \in \Lambda} \left(\mathcal{L}^{(0)}(n) + a\mathcal{L}^{(1)}(n) + a^2 \mathcal{L}^{(2)}(n) + \ldots \right), \tag{2.37}$$

where $\mathcal{L}^{(0)}(n)$ is the Lagrangian for the Wilson action. Since the action has to be dimensionless the improvement terms $\mathcal{L}^{(k)}$ have to be of dimension length $l^{-(4+k)}$.
Sheikholeslami and Wohlert have shown [28] that $\mathcal{O}(a)$ improvement can be achieved by adding a term (see also the discussion in [29])

$$\mathcal{L}^{(1)}(n) = c_{SW} \frac{i}{4} \sum_{\mu<\nu} \underbrace{\overline{\Psi}(n)}_{\propto l^{-3/2}} \sigma_{\mu\nu} \underbrace{\hat{F}_{\mu\nu}(n)}_{\propto l^{-2}} \underbrace{\Psi(n)}_{\propto l^{-3/2}}, \tag{2.38}$$

where c_{sw} is a real coefficient, $\sigma_{\mu\nu} = \frac{i}{2}[\gamma_\mu, \gamma_\nu]$ and $\hat{F}_{\mu\nu}(n)$ is the lattice form of the field strength tensor

$$\hat{F}_{\mu\nu}(n) = \frac{1}{8a^2}\{Q_{\mu\nu}(n) - Q_{\nu\mu}(n)\}\,. \tag{2.39}$$

In (2.39), $Q_{\mu\nu}$ is the sum of 4 plaquettes,

$$Q_{\mu\nu}(n) = U_{\mu\nu}(n) + U_{\nu(-\mu)}(n) + U_{(-\mu)(-\nu)}(n) + U_{(-\nu)\mu}(n)\,. \tag{2.40}$$

According to the form of $Q_{\mu\nu}$, which is shown in figure 2.3, the Sheikholeslami-Wohlert term is also called clover term.

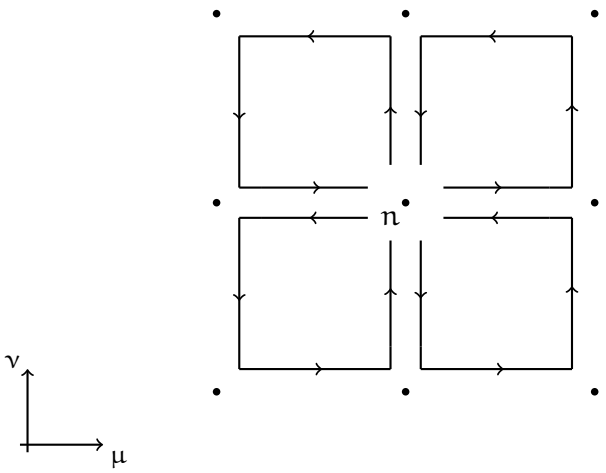

Figure 2.3: Clover Term $Q_{\mu\nu}$

The real coefficient c_{sw} has to be adjusted for each lattice spacing a to remove lattice artifacts [29]. This can also be done at a non-perturbative level [30].

In total the $\mathcal{O}(a)$ improved action S_{sw} is

$$\boxed{S_{sw} = S_w + c_{sw}a^5 \sum_{n\in\Lambda} \frac{i}{4} \sum_{\mu<\nu} \overline{\Psi}(n)\sigma_{\mu\nu}\hat{F}_{\mu\nu}(n)\Psi(n)} \tag{2.41}$$

with the Wilson action S_w from (2.34).

2.6 CORRELATION FUNCTIONS AND WICK'S THEOREM

To calculate matrix elements for pion form factors such as (1.17) and (1.18), one needs to consider two- and three-point correlation functions. In this section we will derive Wick's theorem, which can be used to calculate n-point functions. In section 6.2 we will show how the form factors can be extracted from the two- and three-point correlation functions.

In the path integral formalism an Euclidean correlation function on the lattice can be written as

$$\langle O_1 O_2\rangle = \frac{1}{Z}\int \mathcal{D}[\Psi,\overline{\Psi}]\mathcal{D}[U]\, e^{-S_E[\Psi,\overline{\Psi},U]}\, O_2[\Psi,\overline{\Psi},U]O_1[\Psi,\overline{\Psi},U] \tag{2.42}$$

with the partition function

$$Z = \int \mathcal{D}[\Psi, \overline{\Psi}] \mathcal{D}[U] \, e^{-S_E[\Psi, \overline{\Psi}, U]} \, . \tag{2.43}$$

Since the action S_E is a sum of a fermionic $S_F[\Psi, \overline{\Psi}, U]$ and a gluonic $S_G[U]$ action, (2.42) can be separated in a fermionic and a gluonic part.

$$\langle O_1 O_2 \rangle = \langle \langle O_1 O_2 \rangle_F \rangle_G \tag{2.44}$$

The fermionic expectation value is given by

$$\langle O_1 O_2 \rangle_F = \frac{1}{Z_F[U]} \int \mathcal{D}[\Psi, \overline{\Psi}] \, e^{-S_F[\Psi, \overline{\Psi}, U]} \, O_2[\Psi, \overline{\Psi}, U] O_1[\Psi, \overline{\Psi}, U] \tag{2.45}$$

with

$$Z_F[U] = \int \mathcal{D}[\Psi, \overline{\Psi}] \, e^{-S_F[\Psi, \overline{\Psi}, U]} \, . \tag{2.46}$$

The gluonic part is defined as

$$\langle B \rangle_G = \frac{1}{Z} \int \mathcal{D}[U] \, e^{-S_G[U]} \, Z_F[U] B[U], \tag{2.47}$$

so that $\langle B \rangle_G = \langle O_1 O_2 \rangle$ for $B = \langle O_1 O_2 \rangle_F$.

If one wants to calculate the fermionic expectation value of a product of spinor fields

$$\left\langle \Psi_{n_1} \Psi_{n_2} \cdots \Psi_{n_N} \overline{\Psi}_{m_1} \cdots \overline{\Psi}_{m_N} \right\rangle_F , \tag{2.48}$$

one has to consider that, due to Fermi statistics, interchanging two fermion fields produces a minus sign. Such anticommuting numbers are called Grassmann variables. Some properties of Grassmann numbers[2] are

$$\eta_i \eta_j = -\eta_j \eta_i \quad \Rightarrow \quad \eta_i^2 = 0 \tag{2.49}$$

$$\int d\eta_i 1 = 0 \qquad \int d\eta_i \, \eta_i = 1 \, . \tag{2.50}$$

First of all we want to calculate the fermionic partition function

$$Z_F = \int d\Psi_k d\overline{\Psi}_k \cdots d\Psi_1 d\overline{\Psi}_1 \, \exp\left(\sum_{i,j=1}^{k} \overline{\Psi}_i M_{ij} \Psi_j \right) \, . \tag{2.51}$$

With $M = -a^4 D$ the exponent of (2.51) is the fermionic action $S_F[\Psi, \overline{\Psi}, U]$. Now a transformation of variables

$$\Psi'_j = \sum_{m=1}^{k} M_{jm} \Psi_m \tag{2.52}$$

can be performed. The measure of the integral transforms as

$$d\Psi_k d\overline{\Psi}_k \cdots d\Psi_1 d\overline{\Psi}_1 = \det[M] \, d\Psi'_k d\overline{\Psi}_k \cdots d\Psi'_1 d\overline{\Psi}_1 \, . \tag{2.53}$$

2 An introduction to Grassmann numbers can be found for example in [2] or [19].

Inserting (2.52) and (2.53) in (2.51), one obtains

$$\begin{aligned} Z_F &= \det[M] \int d\Psi'_k d\overline{\Psi}_k \cdots d\Psi'_1 d\overline{\Psi}_1 \, \exp\left(\sum_{i=1}^{k} \overline{\Psi}_i \Psi'_i\right) \\ &= \det[M] \prod_{i=1}^{k} \int d\Psi'_i d\overline{\Psi}_i \exp\left(\overline{\Psi}_i \Psi'_i\right) . \end{aligned} \tag{2.54}$$

Due to (2.49), the Taylor series of the exponential in (2.54) stops after the first two terms. Therefore the fermionic partition function is

$$Z_F = \det[M] \prod_{i=1}^{k} \int d\Psi'_i d\overline{\Psi}_i \left(1 + \overline{\Psi}_i \Psi'_i\right) = \det[M], \tag{2.55}$$

where in the last step (2.50) was used. $\det[M]$ is the so-called fermion determinant.

Now one can calculate the expectation value $\langle \Psi_n \overline{\Psi}_m \rangle_F$.

$$\langle \Psi_n \overline{\Psi}_m \rangle_F = \frac{1}{Z_F} \int d\Psi_k d\overline{\Psi}_k \cdots d\Psi_1 d\overline{\Psi}_1 \, \Psi_n \Psi_m \, \exp\left(\sum_{i,j=1}^{k} \overline{\Psi}_i M_{ij} \Psi_j\right) \tag{2.56}$$

Inserting the transformation (2.52) and applying the Taylor series to the exponential, one obtains

$$\langle \Psi_n \overline{\Psi}_m \rangle_F = \sum_{h=1}^{k} M^{-1}_{nh} \int \prod_{i=1}^{k} d\Psi'_i d\overline{\Psi}_i \underbrace{\prod_{j=1}^{k} (1 + \overline{\Psi}_j \Psi'_j)}_{= \exp\left(\sum_{j=1}^{k} \overline{\Psi}_j \Psi'_j\right)} \Psi'_h \overline{\Psi}_m, \tag{2.57}$$

where $1/Z_F$ has been cancelled by the factor $\det[M]$ from the transformation of the $d\Psi$. Due to $\eta_i^2 = 0$ and $\int d\eta_i 1 = 0$ the integral in (2.57) only does not vanish if the integrand is a product that contains each Ψ' and $\overline{\Psi}$ exactly once. This only is possible for $h = m$ and the one summand of $\prod(1 + \overline{\Psi}_j \Psi'_j)$ where Ψ'_m and $\overline{\Psi}_m$ are missing. Additionally Ψ'_m and $\overline{\Psi}_m$ have to change positions producing a minus sign. Since pairs of Grassmann variables commute the pair $\overline{\Psi}_m \Psi'_m$ can be brought to the position where it is missing. For the expectation value $\langle \Psi_n \overline{\Psi}_m \rangle_F$ one obtains

$$\begin{aligned} \langle \Psi_n \overline{\Psi}_m \rangle_F &= -M^{-1}_{nm} \int d\Psi'_k d\overline{\Psi}_k \cdots d\Psi'_1 d\overline{\Psi}_1 \; \overline{\Psi}_1 \Psi'_1 \cdots \overline{\Psi}_k \Psi'_k \\ &= -M^{-1}_{nm} = a^{-4} D^{-1}_{nm} . \end{aligned} \tag{2.58}$$

Thus the propagator $\langle \Psi_n \overline{\Psi}_m \rangle_F$ is the inverse of the Dirac operator D^{-1}_{nm}. It describes the propagation of a fermion from lattice point n to lattice point m.

(2.58) can be generalised to the N-point function $\langle \Psi_{n_1} \Psi_{n_2} \cdots \Psi_{n_N} \overline{\Psi}_{m_1} \cdots \overline{\Psi}_{m_N} \rangle_F$

$$\begin{aligned} &\langle \Psi_{n_1} \cdots \Psi_{n_N} \overline{\Psi}_{m_1} \cdots \overline{\Psi}_{m_N} \rangle_F \\ &\qquad = (-1)^N \sum_{\mathcal{P}(1,\ldots,n)} \operatorname{sign}(\mathcal{P}) \left(M^{-1}\right)_{n_1 m_{\mathcal{P}_1}} \cdots \left(M^{-1}\right)_{n_N m_{\mathcal{P}_N}} , \end{aligned} \tag{2.59}$$

where a sum over all permutations $\mathcal{P}$ is performed. This is equivalent to a sum over all possible contractions. (2.59) is known as Wick's theorem

As an example we will consider the correlator

$$\left\langle \overline{\Psi}(n)\Gamma\Psi(n)\overline{\Psi}(m)\Gamma\Psi(m)\right\rangle_F = \left\langle \overline{\Psi}_{\alpha,a}(n)\Gamma_{\alpha\beta}\Psi_{\beta,a}(n)\overline{\Psi}_{\gamma,b}(m)\Gamma_{\gamma\delta}\Psi_{\delta,b}(m)\right\rangle_F , \tag{2.60}$$

where all Ψ and $\overline{\Psi}$ have the same quark flavour. Greek letters denote Dirac and Latin letters colour indices. For the indices the Einstein summation convention is used. Γ is one of the 16 Dirac matrices $\Gamma = \{\mathbb{1}, \gamma_\mu, \gamma_5, \gamma_\mu\gamma_5, \sigma_{\mu\nu}\}$. In (2.60) two Wick contractions are possible:

$$\begin{aligned} &\left\langle \overline{\Psi}_{\alpha,a}(n)\Gamma_{\alpha\beta}\Psi_{\beta,a}(n)\overline{\Psi}_{\gamma,b}(m)\Gamma_{\gamma\delta}\Psi_{\delta,b}(m)\right\rangle_F \\ &+\left\langle \overline{\Psi}_{\alpha,a}(n)\Gamma_{\alpha\beta}\Psi_{\beta,a}(n)\overline{\Psi}_{\gamma,b}(m)\Gamma_{\gamma\delta}\Psi_{\delta,b}(m)\right\rangle_F . \end{aligned} \tag{2.61}$$

After interchanging the spinors and performing the contractions one obtains

$$\begin{aligned} \left\langle \overline{\Psi}(n)\Gamma\Psi(n)\overline{\Psi}(m)\Gamma\Psi(m)\right\rangle_F &= -M^{-1}(m,n)_{\delta\alpha,ba}\Gamma_{\alpha\beta}M^{-1}(n,m)_{\beta\gamma,ab}\Gamma_{\gamma\delta} \\ &\quad + M^{-1}(n,n)_{\beta\alpha,aa}\Gamma_{\alpha\beta}M^{-1}(m,m)_{\delta\gamma,bb}\Gamma_{\gamma\delta} \\ &= -\operatorname{Tr}_{CD}\left[M^{-1}(m,n)\Gamma M^{-1}(n,m)\Gamma\right] \\ &\quad + \operatorname{Tr}_{CD}\left[M^{-1}(n,n)\Gamma\right]\operatorname{Tr}_{CD}\left[M^{-1}(m,m)\Gamma\right], \end{aligned} \tag{2.62}$$

where Tr_{CD} denotes a trace in colour- and Dirac-space. The first summand of (2.62) is quark connected, while the second summand is quark disconnected. The two contributions are shown in figure 2.4.

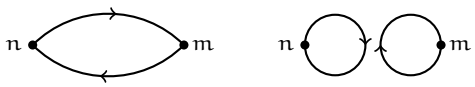

Figure 2.4: Connected part on the left-hand side, disconnected on the right

In general, all diagrams with quark lines that are not connected to each other are called quark disconnected.

So far we did not consider the gauge expectation value, which has also to be calculated. Therefore one creates gauge configurations U_n. A gauge configuration is a collection of link variables $U_\mu(n)$ for all links in the lattice. A set of gauge configurations is called an ensemble. In an ensemble the gauge configurations U_n are distributed with a probability proportional to the weight $\exp(-S_G[U_n])$. Therefore the gauge expectation value can be approximated by calculating the mean over the N different gauge configurations of an ensemble

$$\langle O\rangle = \frac{1}{Z}\int \mathcal{D}[U]e^{-S_G[U]}O[U] \approx \frac{1}{N}\sum_{n=1}^{N} O[U_n] . \tag{2.63}$$

The configurations are generated in a Markov chain [31]

$$U_\mu(x)_0 \to U_\mu(x)_1 \to U_\mu(x)_2 \to \dots \tag{2.64}$$

In each step the configuration is either accepted or rejected due to its weight by the Metropolis algorithm [32]. An overview of the whole procedure of generating ensembles can be found for example in [19].

3

INVERSION ALGORITHMS

3.1 POINT SOURCES

According to Wick's theorem (2.59), one has to invert the Dirac operator to calculate an n-point function of fermions. On the lattice this requires an inversion of a $12M \times 12M$ matrix[1], where $M = L^3 \times T$ is the total number of lattice points. For many applications it is sufficient to calculate so called point-to-all propagators, which describe the propagation of a quark from a fixed point m to an arbitrary point on the lattice. To obtain a point-to-all propagator the corresponding column of the inverse Dirac matrix is needed. This can be calculated using point sources. Therefore the point source has to be placed at point m and one has to solve the Dirac equation

$$D|s\rangle = (0, \ldots, 0, 1, 0, \ldots, 0)^T \,. \tag{3.1}$$

This calculation has to be repeated for all combinations of Dirac- and colour-indices. Therefore 12 equations of the type (3.1) have to be solved to obtain a point-to-all propagator.

3.2 INVERSION WITH STOCHASTIC SOURCES

For the calculation of the scalar pion form factor (and also other quantities) one is interested in diagrams containing a disconnected quark loop, i.e. a quark that propagates from an arbitrary lattice point to the same point.

$$\sum_n \mathrm{Tr}_{CD}\left[M^{-1}(n,n)\Gamma\right] = \mathrm{Tr}\left[M^{-1}\Gamma\right] \tag{3.2}$$

Thus a calculation with point sources is very expensive, since it requires to solve the Dirac equation $12 \cdot L^3 \times T$ times. To avoid this, one can use stochastic sources [8, 9, 33]. For this method N random vectors $|\eta^i\rangle$ with $i = \{1, \ldots, N\}$ are needed, where N can be chosen small ($N \ll 12 \cdot L^3 \times T$). The random vectors $|\eta^i\rangle$ have to fulfil the properties

$$\frac{1}{N}\sum_{i=1}^{N} |\eta^i\rangle = \mathcal{O}\left(1/\sqrt{N}\right), \qquad \text{and} \tag{3.3a}$$

$$\frac{1}{N}\sum_{i=1}^{N} |\eta^i\rangle\langle\eta^i| = \mathbb{1} + \mathcal{O}\left(1/\sqrt{N}\right) . \tag{3.3b}$$

1 12 because of the four Dirac and the three colour components

Now one has to (numerically) solve the N sets of linear equations

$$D|s^i\rangle = |\eta^i\rangle, \tag{3.4}$$

where D is the lattice Dirac operator, so D^{-1} is the propagator of interest. This results in

$$\begin{aligned} |s^i\rangle &= D^{-1}|\eta^i\rangle \\ \Rightarrow |s^i\rangle\langle\eta^i| &= D^{-1}|\eta^i\rangle\langle\eta^i| \\ \Rightarrow \frac{1}{N}\sum_{i=1}^{N}|s^i\rangle\langle\eta^i| &= D^{-1}\underbrace{\frac{1}{N}\sum_{i=1}^{N}|\eta^i\rangle\langle\eta^i|}_{\approx\mathbb{1}} \\ &\approx D^{-1}, \end{aligned} \tag{3.5}$$

where one makes use of (3.3b) in the last step. Therefore

$$\boxed{D^{-1} = \frac{1}{N}\sum_{i=1}^{N}|s^i\rangle\langle\eta^i|} \tag{3.6}$$

is an estimate for the propagator D^{-1}. (3.6) implies that D^{-1} can be calculated as the average over $|s^i\rangle\langle\eta^i|$ for all stochastic sources $|\eta^i\rangle$.

In the following sections some methods discussed in [9] will be introduced, which either reduce the stochastic error on D^{-1} or the computer time needed for the calculation.

3.3 DILUTION

For dilution [34] the vector space $\mathcal{R}$ = lattice sites $\otimes$ colour $\otimes$ spin is decomposed into m subspaces $\mathcal{R}_j$.

$$\mathcal{R} = \bigoplus_{j=1}^{m}\mathcal{R}_j \tag{3.7}$$

Now the N source vectors $|\eta^i_{|j}\rangle$ are set to zero outside the subspace $\mathcal{R}_j$. The solutions of (3.4) with $|\eta^i\rangle = |\eta^i_{|j}\rangle$ are called $|s^i_{|j}\rangle$. The propagator then is computed by

$$D^{-1} = \sum_{j=1}^{m}\frac{1}{N}\sum_{i=1}^{N}|s^i_{|j}\rangle\langle\eta^i_{|j}|\,. \tag{3.8}$$

Some possibilities for dilution are:

TIME DILUTION: The sources only have non-vanishing entries for one timeslice.

EVEN-ODD DILUTION: The sources only have non-vanishing entries for lattice sites n where the sum $n_0+n_1+n_2+n_3$ is even for one subspace and odd for the other one.

One can also have non vanishing entries only on the even or odd points in one timeslice, which is a combination of even-odd and time dilution.

SPIN DILUTION: The sources only have non-vanishing entries for one Dirac component.

COLOUR DILUTION: The sources only have non-vanishing entries for one colour component.

3.4 THE HOPPING PARAMETER EXPANSION

The Hopping Parameter Expansion (HPE) as described in [9] is suitable for matrices of the form

$$\begin{aligned} 2\kappa \cdot D &= \mathbb{1} - \kappa \cdot H \\ \Rightarrow D &= \frac{1}{2\kappa}\,\mathbb{1} - \frac{1}{2}\,H \end{aligned} \tag{3.9}$$

like the Klein-Gordon operator (2.11) or the unimproved Wilson-Dirac operator (2.31). For the Dirac operator the unit matrix $\mathbb{1}$ in (3.9) is a unit matrix in space-time, Dirac-space and colour-space $\mathbb{1}_{N\times N} \otimes \mathbb{1}_{4\times 4} \otimes \mathbb{1}_{3\times 3}$. H only has entries that link neighbouring lattice points. The propagator can be written as

$$D^{-1} = \left(\frac{1}{2\kappa}\,\mathbb{1} - \frac{1}{2}\,H\right)^{-1} . \tag{3.10}$$

If one applies a geometrical series to (3.10), one obtains

$$D^{-1} = 2\kappa \sum_{i=0}^{\infty} (\kappa H)^i \tag{3.11a}$$

$$= 2\kappa \sum_{i=0}^{k-1} (\kappa H)^i + 2\kappa \sum_{i=k}^{\infty} (\kappa H)^i . \tag{3.11b}$$

(3.11a) implies that the entry $D^{-1}(n, m)$ of the propagator can be seen as a sum over all possible paths from n to m [19]. A path of the length i is suppressed by a power κ^i of the hopping parameter.

(3.11b) can be rewritten as

$$D^{-1} = 2\kappa \sum_{i=0}^{k-1} (\kappa H)^i + (\kappa H)^k \cdot D^{-1} . \tag{3.12}$$

On the right-hand side of (3.12) D^{-1} can be replaced by the inverse calculated using stochastic sources (3.6).

$$\boxed{D^{-1} = 2\kappa \sum_{i=0}^{k-1} (\kappa H)^i + (\kappa H)^k \cdot \frac{1}{N} \sum_{i=1}^{N} |s^i\rangle\langle\eta^i|} \tag{3.13}$$

The idea of the hopping parameter expansion is to calculate the shortest paths, which are the largest contributions to D^{-1}, explicitly and to estimate the remaining terms with stochastic sources. Thus one expects the stochastic error of the propagator to decrease when using the HPE. When the hopping parameter κ is

small, the influence of the longer paths decreases and the HPE is expected to converge faster.

For the Wilson-Dirac operator the hopping matrix has the form

$$\begin{aligned} H_W(n,m) &= \sum_{\mu=0}^{3} \left(U_\mu(n)(1-\gamma_\mu)\delta_{n+a\mu,m} + U_{-\mu}(n)(1+\gamma_\mu)\delta_{n-a\mu,m} \right) \\ &= \sum_{\mu=\pm 0}^{\pm 3} U_\mu(n)(1-\gamma_\mu)\delta_{n+a\mu,m} \end{aligned} \tag{3.14}$$

with

$$\gamma_{-\mu} \equiv -\gamma_\mu \,. \tag{3.15}$$

To calculate disconnected loops, the trace $\mathrm{Tr}\left(\Gamma \cdot D^{-1}\right)$ has to be taken. If the hopping parameter expansion (3.13) is used, one needs the trace of the powers of the hopping matrix (3.14). Trivially the trace of all odd powers vanish since it is not possible to jump from one lattice point to the same point with an odd number of jumps. Therefore one only has to look at the even powers of the hopping matrix. $H_W^0(n,m)$ is just a unit matrix in space-time, colour and Dirac space. Therefore $\mathrm{Tr}\left(\Gamma \cdot H_W^0(n,m)\right) = \mathrm{Tr}\left(\Gamma \cdot \mathbb{1}_{12N\times 12N}\right) = 0$ except for $\Gamma = \mathbb{1}$ where the calculation of the trace is trivial.
For the second power $H_W^2(n,m)$ one obtains [19]

$$H_W^2(n,m) = \sum_{\mu,\nu=\pm 0}^{\pm 3} (1-\gamma_\mu)(1-\gamma_\nu) U_\mu(n) U_\nu(n+a\mu) \delta_{n+a\mu+a\nu,m}. \tag{3.16}$$

If one takes the trace $\mathrm{Tr}\left(\Gamma \cdot H_W^2(n,m)\right)$, ν has to be $-\mu$ because of $\delta_{n+a\mu+a\nu,n}$, which means jumping to a neighbouring point and jumping back again. But doing so one gets in (3.16)

$$(1-\gamma_\mu)(1+\gamma_\mu) = 0 \,. \tag{3.17}$$

Thus jumping backwards to get back to the starting point is not allowed.
In the forth power of $H_W(n,m)$, one can jump around a plaquette from a lattice point to the same point. Therefore $\mathrm{Tr}\left(\Gamma \cdot H_W^4(n,m)\right) \neq 0$ for $\Gamma = \{\mathbb{1}, \gamma_5, \sigma_{\mu\nu}\}$. For $\Gamma = \{\gamma_\mu, \gamma_\mu\gamma_5\}$ this trace vanishes due to the trace theorems of the γ-matrices. For γ_μ and $\gamma_\mu\gamma_5$ also $\mathrm{Tr}\left(\Gamma \cdot H_W^6(n,m)\right)$ vanishes.

For the hopping parameter expansion (3.12) with the Wilson-Dirac operator it is appropriate to take $k = 4$ for $\Gamma = \{\mathbb{1}, \gamma_\mu, \sigma_{\mu\nu}\}$ and $k = 8$ for $\Gamma = \{\gamma_5, \gamma_\mu\gamma_5\}$ [9].

$$\mathrm{Tr}\left(\Gamma \cdot D^{-1}\right) = \begin{cases} 2\kappa \mathrm{Tr}\left(\mathbb{1}\right) + \kappa^4 \mathrm{Tr}\left(H^4 D^{-1}\right) & \Gamma = \mathbb{1} \\ \kappa^4 \mathrm{Tr}\left(\Gamma \cdot H^4 D^{-1}\right) & \Gamma = \{\gamma_\mu, \sigma_{\mu\nu}\} \\ \kappa^8 \mathrm{Tr}\left(\Gamma \cdot H^8 D^{-1}\right) & \Gamma = \{\gamma_5, \gamma_\mu\gamma_5\} \end{cases} \tag{3.18}$$

HPE with clover Term

The $\mathcal{O}(a)$-improved Wilson-Dirac operator (2.41) does not have the form (3.9). Its form is

$$D_{sw} = \frac{1}{2\kappa}\mathbb{1}_{12N\times 12N} + c_{sw}B - \frac{1}{2}H \tag{3.19}$$

with a real constant c_{sw} and

$$B = a\,\frac{i}{4}\sigma_{\mu\nu}\hat{F}_{\mu\nu}\,. \tag{3.20}$$

B contains a unit matrix $\mathbb{1}_{N\times N}$ in space-time but not in Dirac-space (due to $\sigma_{\mu\nu}$) and in colour-space (due to $\hat{F}_{\mu\nu}$). The complete diagonal part of D_{sw} is no longer proportional to the unit matrix $\mathbb{1}_{12N\times 12N}$ when adding the clover term. Therefore the hopping parameter expansion as described above cannot be used.

The hopping parameter expansion can be adapted to the $\mathcal{O}(a)$-improved Wilson-Dirac as follows.

At first (3.19) has to be rewritten as

$$D_{sw} = A - \frac{1}{2}H \tag{3.21}$$

$$\text{with} \qquad A = \frac{1}{2\kappa}\mathbb{1} + c_{sw}B = \left(m + \frac{4}{a}\right)\mathbb{1} + c_{sw}B\,. \tag{3.22}$$

The matrix A can now be factored out.

$$D_{sw} = A(\mathbb{1} - \frac{1}{2}A^{-1}H)$$

This way one obtains for the inverse of the $\mathcal{O}(a)$-improved Wilson-Dirac operator

$$D_{sw}^{-1} = (\mathbb{1} - \frac{1}{2}A^{-1}H)^{-1}A^{-1}\,. \tag{3.23}$$

The left factor of (3.23) can now be calculated using a geometrical series as done for the hopping parameter expansion.

$$\begin{aligned}\left(\mathbb{1} - \frac{1}{2}A^{-1}H\right)^{-1} &= \sum_{i=0}^{\infty}\left(\frac{1}{2}A^{-1}H\right)^{i} \\ &= \sum_{i=0}^{k-1}\left(\frac{1}{2}A^{-1}H\right)^{i} + \left(\frac{1}{2}A^{-1}H\right)^{k}\left(\mathbb{1} - \frac{1}{2}A^{-1}H\right)^{-1}\end{aligned} \tag{3.24}$$

To obtain the inverse of the $\mathcal{O}(a)$-improved Wilson-Dirac operator one has to insert (3.24) in (3.23).

$$\begin{aligned}D_{sw}^{-1} &= (\mathbb{1} - \frac{1}{2}A^{-1}H)^{-1}A^{-1} \\ &= \sum_{i=0}^{k-1}\left(\frac{1}{2}A^{-1}H\right)^{i}A^{-1} + \left(\frac{1}{2}A^{-1}H\right)^{k}D_{sw}^{-1}\end{aligned} \tag{3.25}$$

D_{SW}^{-1} on the right-hand side of (3.25) can now be replaced by the inverse of the $\mathcal{O}(a)$-improved Wilson-Dirac operator calculated using stochastic sources.

To calculate the hopping parameter expansion (3.25) with clover term, one additionally has to invert the matrix A which was defined by (3.22)

$$A = \left(m + \frac{4}{a}\right) + c_{SW}\, a\, \frac{i}{4}\sigma_{\mu\nu}\hat{F}_{\mu\nu}\,. \tag{3.26}$$

Using the definition of the Euklidean gamma matrices in chiral representation (see (2.8)), one obtains the following block diagonal form in Dirac space [35]

$$A = \begin{pmatrix} \tilde{A}_+ & 0 \\ 0 & \tilde{A}_- \end{pmatrix} \tag{3.27}$$

with the 6×6 matrices

$$\tilde{A}_\pm = \left(\frac{4}{a} + m + c_{SW}\frac{i}{16}\sum_{k=1}^{3}\sigma_k\left(\mathcal{E}_k \mp \mathcal{B}_k\right)\right)\,. \tag{3.28}$$

$\mathcal{E}_k$ and $\mathcal{B}_k$ are the electric and magnetic components of the field strength tensor,

$$\mathcal{E}_k = 8\hat{F}_{0k}\,, \qquad \mathcal{B}_k = \sum_{i,j=1}^{3} 4\epsilon_{ijk}\hat{F}_{ij}\,. \tag{3.29}$$

Due to the block structure of A, for the calculation of A^{-1} two 6×6 matrices $\tilde{A}_\pm$ have to be inverted for every lattice point.

3.5 THE TRUNCATED SOLVER METHOD

The truncated solver method (TSM) [36] is a method to reduce the computational costs of the calculation of the propagator. The idea of TSM is to solve equations (3.4) for N random sources using a lower number n_t of solver iterations. The obtained solutions are called $|s^i_{(n_t)}\rangle$. Additionally more exact solutions $|s^i\rangle$ are calculated for a small subset of these sources. The propagator is then calculated by

$$D^{-1} = \frac{1}{N_1}\sum_{i=1}^{N_1}|s^i_{(n_t)}\rangle\langle\eta^i| + \frac{1}{N_2}\sum_{i=N_1+1}^{N_1+N_2}\left(|s^i\rangle - |s^i_{(n_t)}\rangle\right)\langle\eta^i| \tag{3.30}$$

with the number N_1 of sources for which only the inexact solution is calculated and the number $N_2 = N - N_1$ of sources for which unexact and more exact solutions are calculated. The second summand in (3.30) can be seen as a correction to the inverse calculated only with the solutions $|s^i_{(n_t)}\rangle$.

4

THE KLEIN-GORDON OPERATOR IN TWO DIMENSIONS

In this section as a toy model the free Klein-Gordon propagator will be calculated using stochastic sources. The calculation will be performed on a two-dimensional 10×10 lattice, thus in one time and one spatial dimension. It will be tested whether or not dilution, HPE and TSM improve the calculation.
According to (2.11)

$$D_{KG}\Phi(n) = \frac{m^2a^2 + 2d}{a^2}\Phi(n) - \sum_{\mu=0}^{d}\frac{1}{a^2}\left(\Phi(n + a\mu) + \Phi(n - a\mu)\right)$$

the Klein-Gordon operator on the 10×10 lattice can be written as a 100×100 matrix since the lattice has in total 100 lattice points. The entry D_{ij} with $i, j = 1, \ldots, 100$ of the Klein-Gordon matrix denotes the link between lattice point i and lattice point j. For our two-dimensional ($d = 2$) toy model we will use $m = 1$ and $a = 1$, thus the matrix associated with the Klein-Gordon operator is

$$D_{ij} = \begin{cases} 5 & i = j \\ -1 & i \text{ neighbouring point of } j \\ 0 & \text{otherwise.} \end{cases} \tag{4.1}$$

In the following we will use periodic boundary conditions. Thus the last lattice point in one dimension is a direct neighbour of the first point in the same dimension. An example for a 10×10 lattice with periodic boundary conditions is shown in figure 4.1.

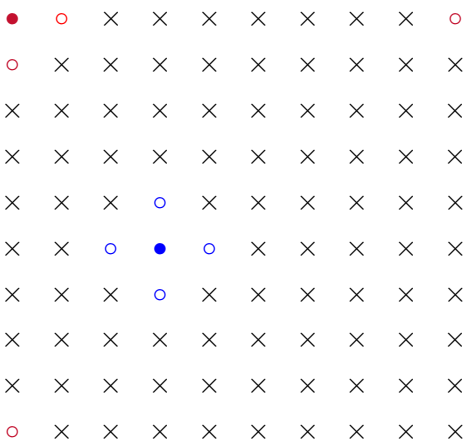

Figure 4.1: 2-dimensional 10×10 lattice with periodic boundary conditions: The points marked with $\circ$ are the neighbours of those marked with $\bullet$ in the same colour.

To calculate the propagator, the 100×100 matrix (4.1) has to be inverted.

4.1 INVERSION WITH STOCHASTIC SOURCES

For the inversion of the Klein-Gordon operator $\mathbb{Z}(2)$ sources were used. Every element of the random vector is either 1 or -1 with a probability of 50% each. These sources fulfil the required properties (3.3a) and (3.3b). The solution of the sets of linear equations

$$D|s^i\rangle = |\eta^i\rangle \tag{4.2}$$

was done using the Biconjugate Gradient method [37]. The Biconjugate Gradient stops when

$$\frac{|D|s\rangle_k - |\eta\rangle|}{||\eta\rangle|} < 0.00001 \tag{4.3}$$

is fulfilled, where $|s\rangle_k$ is the solution after k iterations. For the 10×10 lattice k is about 14 to 15.
To test whether the calculation of the propagator with stochastic sources works, additionally the linear equation

$$D|s'\rangle = (1, 0, \ldots, 0)^T \tag{4.4}$$

was solved with a point source $(1, 0, \ldots, 0)^T$ using the Biconjugate Gradient method. The solution $|s'\rangle$ is the first column of the exact inverse of D.

For calculating the propagator 1000 stochastic sources were used, thus the inverse of the Klein-Gordon operator can be estimated as the average over $|s_i\rangle\langle\eta_i|$ for 1000 $|\eta_i\rangle$. In our case of a 100×100 matrix an exact calculation where only 100 point sources have to be used would require less computer time. However, we want to test the method of stochastic sources for this toy model with a certain amount of sources. Later we will use much larger lattices and the number of stochastic sources will be much smaller than the number of required point sources, which equals the number of lattice points.
The first 10 entries of the first column of the propagator calculated using stochastic sources and calculated exactly are shown in table 4.1.

D^{-1}_{stoch}	D^{-1}_{exact}
0.246271	0.254066
0.062522	0.067582
0.024498	0.019774
0.000174	0.006275
0.009105	0.002279
0.001559	0.001387
-0.013380	0.002279
0.004310	0.006275
0.041162	0.019774
0.051289	0.067582

Table 4.1: The first 10 entries of the first column of the inverse of the Klein-Gordon operator with stochastic sources (D^{-1}_{stoch}) and calculated exactly (D^{-1}_{exact})

In this table one can see that the method of stochastic sources works quite well.

4.2 TESTING DILUTION

Time Dilution

First of all it will be tested if time dilution improves the calculation of the propagator. For time dilution the random sources have to be changed such that only the entries for one timeslice are random numbers. All remaining entries are set to zero. Therefore the lattice points are labelled such that the points for timeslice $n_0 = 0$ come first, then the ones for $n_0 = 1$ and so on. Doing so, the Klein-Gordon operator has a block structure, where in each 10×10 block only lattice points from two certain timeslices are linked. In the blocks on the diagonal all points from the same timeslice are connected. Lattice points that are linked in blocks that are further away from the diagonal blocks of the matrix have a larger distance in time, where periodic boundary conditions have to be taken into account, as depicted in figure 4.2. Since the matrix only couples a lattice point with itself and its direct neighbours, only the blocks on the diagonal and the blocks next to the the diagonal blocks contain entries that are non-zero. All other blocks contain only zeros.

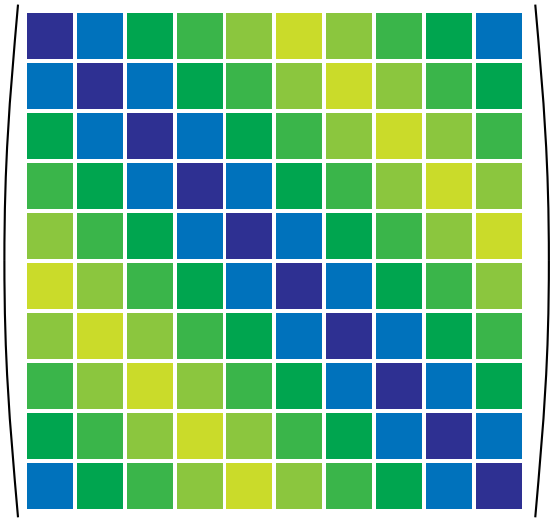

Figure 4.2: Schematic picture of the Klein-Gordon matrix: Every block is a 10×10 matrix. The diagonal blocks in dark blue contain all entries that couple points from the same time, thus a point with itself and with all direct neighbours in spatial directions. The blocks in light blue contain the entries that couple points with a direct neighbour in time direction. The green blocks contain only zeros, since they link points that have a temporal distance which is larger than one in lattice units. The lighter the green of these blocks, the larger is the time distance of the linked lattice points, where periodic boundary conditions are used.

For the 10×10 lattice the time diluted sources look like

$$\begin{aligned} |\eta\rangle &= (\overbrace{\pm 1, \ldots, \pm 1}^{10 \text{ entries}}, \quad 0, \ldots, 0)^T \\ |\eta\rangle &= (\overbrace{0, \ldots, 0}^{10 \text{ entries}}, \overbrace{\pm 1, \ldots, \pm 1}^{10 \text{ entries}}, \quad 0, \ldots, 0)^T \\ &\ldots \end{aligned} \tag{4.5}$$

To have the same computational cost as for the calculation without dilution, 100 sources were used for every timeslice. In total these are $10 \times 100 = 1000$ sources. Therefore 1000 sets of linear equations have to be solved as for the case without dilution.

Now one can compare the first row of the propagator D^{-1}_{timedil} calculated using time dilution with the propagator D^{-1}_{stoch} calculated without time dilution. Since the propagator also has a block structure in time, one can compare the entries block by block. The block structure is illustrated in figure 4.3.

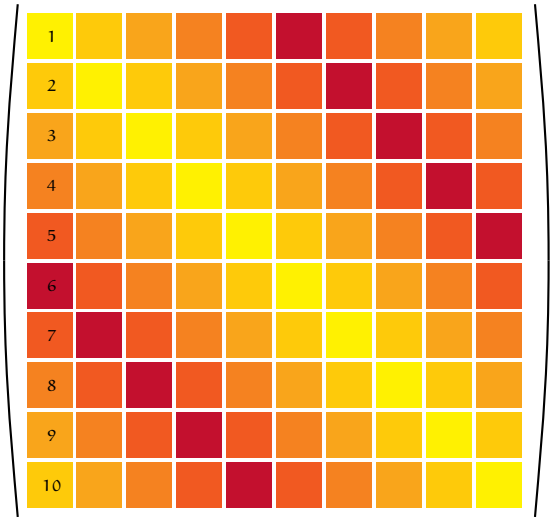

Figure 4.3: Schematic picture of the Klein-Gordon propagator: Every block is a 10×10 matrix. The blocks labelled with 1 to 10 will be used for the comparison of the propagator calculated with and without time dilution. The yellow blocks are the diagonal blocks. The darker the colour of a block the larger is the temporal distance in time.

For the comparison of D^{-1}_{timedil} and D^{-1}_{stoch}, the first column of the propagator is used, thus the first columns of blocks 1 to 10. In figure 4.4 it is shown in how many cases the values for dilution are better.
One can see that for block 1 the difference of D^{-1}_{stoch} and D^{-1}_{exact} in most cases is smaller than the difference between D^{-1}_{timedil} and D^{-1}_{exact}. In block 2 and 10 about half of the entries are closer to the exact value when using time dilution. For the other blocks for most entries D^{-1}_{timedil} is better. Thus time dilution works best for the blocks that are far away from block 1, which is a block on the diagonal of the propagator. If one looks at other columns of the propagator it turns out that time dilution improves the calculation best in the blocks that are farthest away from the diagonal, thus blocks that link lattice points with the largest time separation. For the diagonal blocks, thus blocks that link lattice points from the same timeslice, time dilution does not improve the result. The darker the blocks in figure 4.3 the larger is the distance to the diagonal of the propagator and the better time dilution improves the values.

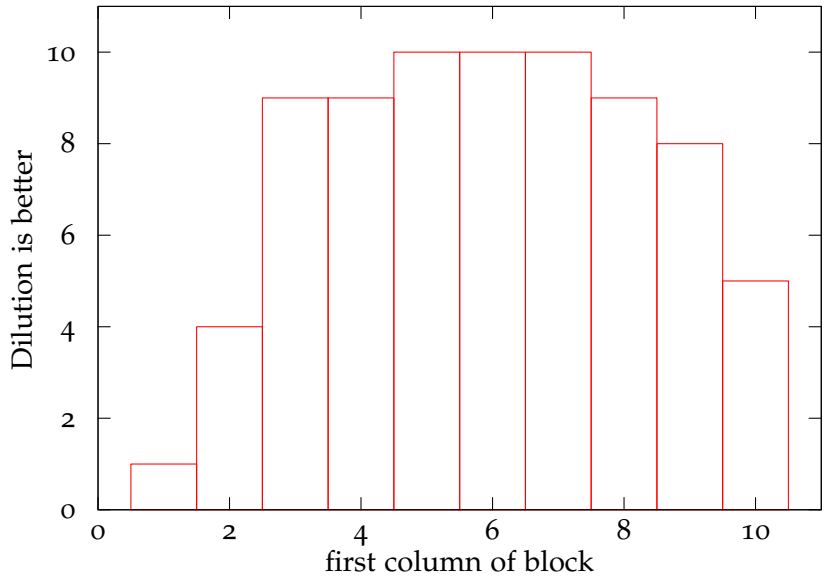

Figure 4.4: Number of entries in the first column of blocks 1 to 10 for which the the value calculated using time dilution is closer to the exact value than the one calculated without time dilution.

In addition the propagator was calculated ten times using different seeds to compare the variances of the values calculated with and without time dilution. Here one can see that the variances show a similar behaviour as the differences to the exact solution. For the blocks on the diagonal the variance of the propagator calculated without time dilution is smaller. For the other blocks the ones with time dilution are better and the variance is the smallest for the blocks that are farthest away from the diagonal, taking periodic boundary conditions into account.

Since for the disconnected loops one needs the trace - and therefore only the diagonal entries - of the propagator, time dilution does not help.

Even-Odd Dilution

With even-odd dilution the stochastic sources look like

$$\begin{aligned} |\eta_e\rangle &= (\overbrace{\pm 1, 0, \pm 1, \ldots, 0}^{10 \text{ entries}}, \overbrace{0, \pm 1, \ldots, \pm 1}^{10 \text{ entries}}, \quad \ldots)^T \\ |\eta_o\rangle &= (\overbrace{0, \pm 1, 0, \ldots, \pm 1}^{10 \text{ entries}}, \overbrace{\pm 1, 0, \ldots, 0}^{10 \text{ entries}}, \quad \ldots)^T . \end{aligned} \tag{4.6}$$

To have the same number of sets of equations as for the calculation without dilution, I used 500 sources for the even and 500 sources for the odd points, which are 1000 sources in total. In figure 4.5 it is plotted for the first column of D^{-1} how many entries of the propagator calculated with even-odd dilution are closer to the exact value than the ones calculated without dilution.

If one compares the propagator calculated with and without even-odd dilution, one can see that the numbers with even-odd dilution are better in about 40% to

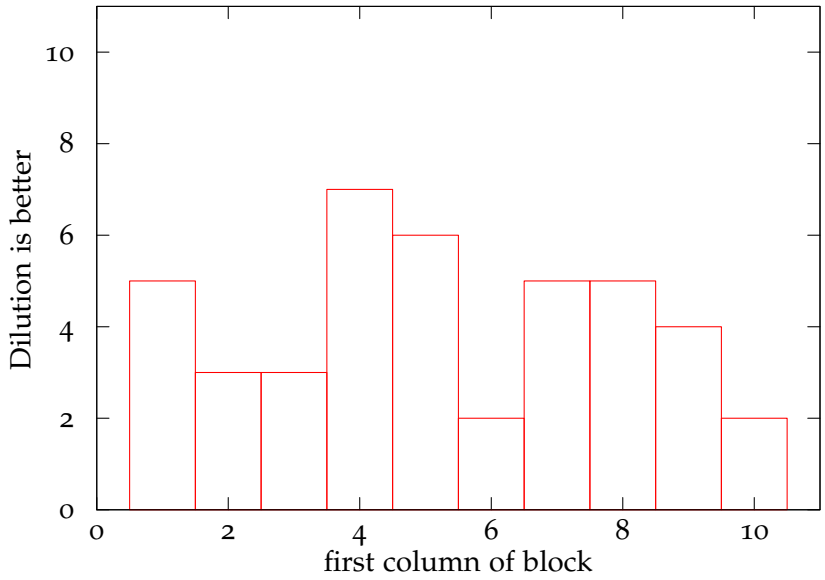

Figure 4.5: How many entries are better with than without even-odd dilution

50% of the cases, whereas the other numbers are better without dilution. Also no dependence of the block of the propagator is observed. Therefore even-odd dilution does not seem to improve the propagator.

4.3 TESTING THE HOPPING PARAMETER EXPANSION

For $a = 1$, $m = 1$ and $d = 2$ the hopping parameter for the Klein-Gordon operator (2.13) is

$$\kappa \equiv \frac{a^2}{2\,(m^2a^2 + 2d)} = \frac{1}{10}\,. \tag{4.7}$$

The Klein-Gordon matrix (4.1) can be split into a matrix proportional to the unit matrix and a hopping matrix H as described in (2.12). The hopping matrix H, which only couples nearest neighbours, is given by

$$H_{ij} = \begin{cases} 2 & i \text{ neighbouring point of } j \\ 0 & \text{otherwise.} \end{cases} \tag{4.8}$$

Now the hopping parameter expansion (3.13)

$$D^{-1} = 2\kappa \sum_{i=0}^{k-1} (\kappa H)^i + (\kappa H)^k \cdot \frac{1}{N} \sum_{i=1}^{N} |s^i\rangle\langle\eta^i| \tag{4.9}$$

can be applied for different numbers of terms k. The first part of the HPE

$$2\kappa \sum_{i=0}^{k-1} (\kappa H)^i \tag{4.10}$$

was calculated explicitly by inserting a unit matrix and applying $(\kappa H)^i$ for every summand in (4.10). For the second part

$$(\kappa H)^k \cdot \frac{1}{N} \sum_{i=1}^{N} |s^i\rangle\langle\eta^i| \tag{4.11}$$

again 1000 random sources $|\eta^i\rangle$ were used.

$k = 0$ is equivalent to calculating only with stochastic sources without performing a hopping parameter expansion and therefore gives the same result as before.

The difference of the (0,0)-component of the propagator from the exact value is shown in figure 4.6 for different numbers of terms k in the HPE.

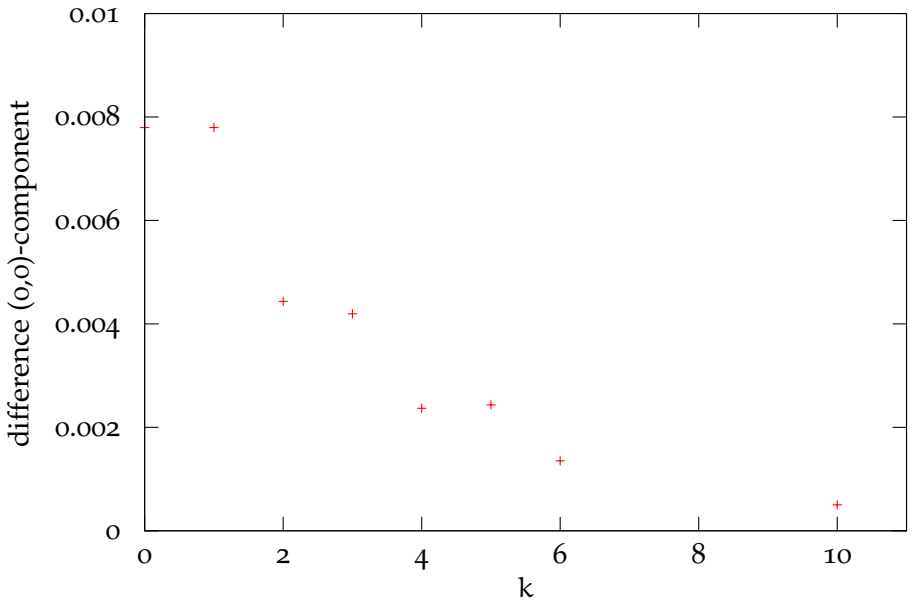

Figure 4.6: Difference of the (0,0)-component between the exact solution and the one calculated with stochastic sources and HPE

As one can see, the difference of the (0,0)-component to the exact solution decreases when more terms in the HPE are calculated. Between an even number of terms and the next odd number (from 0 to 1, from 2 to 3 and so on) the difference nearly stays the same. This is because the diagonal elements of all odd powers of H and therefore all diagonal elements of the odd terms in the hopping parameter expansion vanish. It is not possible to jump from one lattice point to the same point with an odd number of jumps. The variance of the (0,0)-component calculated using ten different seeds, which is shown in figure 4.7, shows a similar behaviour.

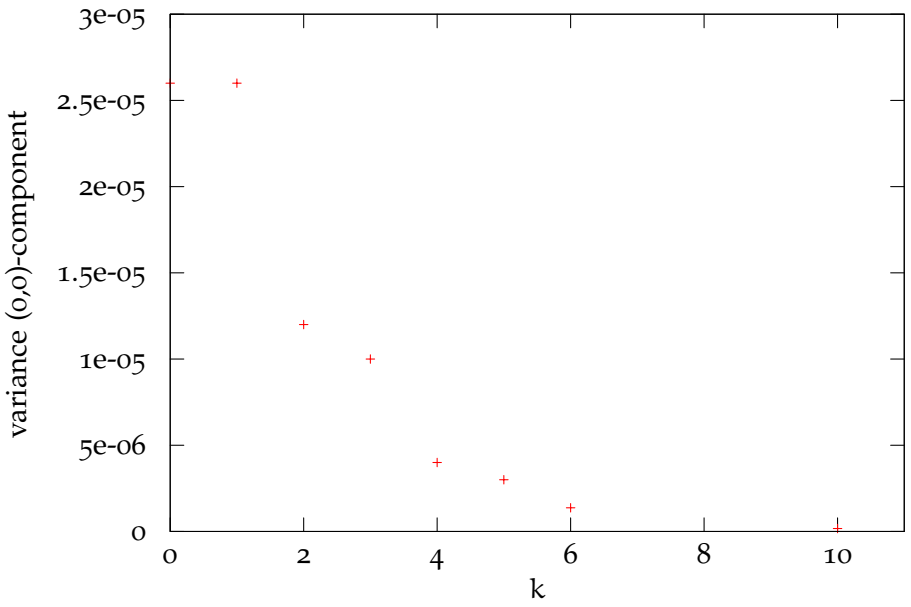

Figure 4.7: Variance of the (0,0)-component of the propagator calculated using stochastic sources and HPE with 10 different seeds

Also for the other components of the propagator the difference to the exact solution and the variance decrease when calculating more terms in the HPE.

Obviously the hopping parameter expansion improves the calculation of the propagator. The difference to the exact solution as well as the variance decreases if more terms of the HPE are calculated. Since for the disconnected loops one is interested in the diagonal elements, one should use an even number of terms since the next odd number does not improve the value of the propagator.

4.4 TESTING THE TRUNCATED SOLVER METHOD

Since the aim of the truncated solver method is a reduction of the computational costs, also the CPU time for the calculation has to be measured. The truncated solver method (3.30)

$$D^{-1} = \frac{1}{N_1}\sum_{i=1}^{N_1} |s^i_{(n_t)}\rangle\langle\eta^i| + \frac{1}{N_2}\sum_{i=N_1+1}^{N_1+N_2}\left(|s^i\rangle - |s^i_{(n_t)}\rangle\right)\langle\eta^i| \tag{4.12}$$

was applied for $N_1 = \{950, 970, 980, 990\}$ with a fixed number of $N_1 + N_2 = 1000$ sources. For the $N_1 + N_2$ solutions $|s^i_{(n_t)}\rangle$ 4, 6, 8 and 10 were used as a maximum number of iterations for the biconjugate gradient. The N_2 more exact solutions $|s^i\rangle$ were calculated with the same condition (4.3) as before which is fulfilled after about 14 or 15 solver iterations.

As expected the CPU time needed for the calculation decreases if fewer iterations are used or fewer solutions N_2 are calculated more exactly. Since the calculation of the propagator is not done as accurately as without the TSM, the differences to the exact solution and the variances get worse using the truncated solver method.

To check if the time reduction is worth the bigger error of the propagator, the variance of the (0,0)-component after 10 calculations times the CPU time needed for the calculation was considered. In figure 4.8 this is plotted for the different values of N_1 against the maximum number of iterations used.

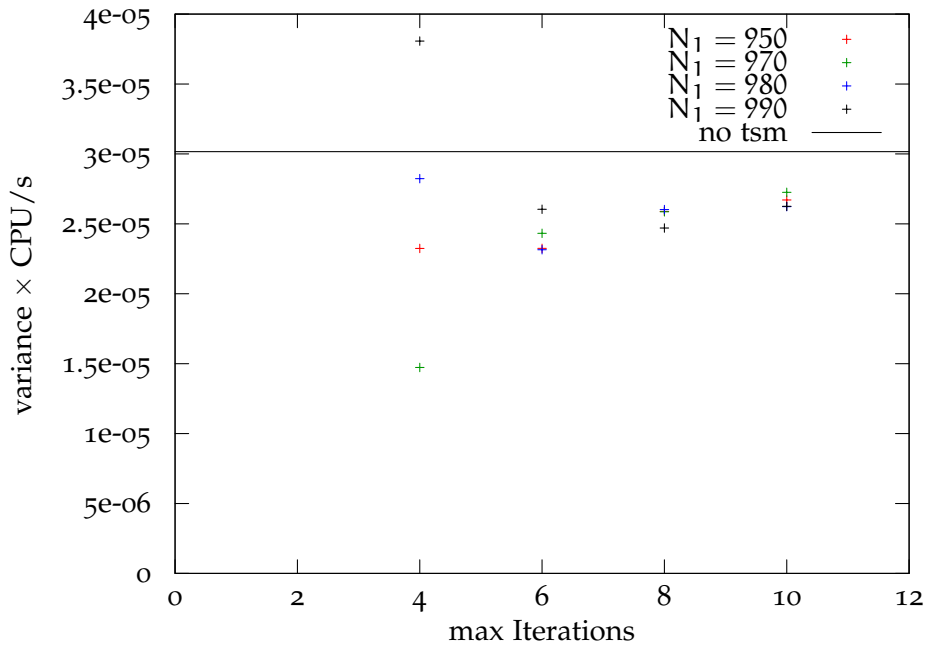

Figure 4.8: TSM: variance of the (0,0) component of the propagator times CPU time used. The horizontal black line shows the value for the calculation that is done only with stochastic sources.

As one can see, the variance times the CPU time is smaller for most combinations of N_1 and maximum numbers of iterations than the value for the calculation without TSM. This means that the reduction of computational costs is bigger than the increase of the variance. The TSM is doing what it was supposed to do. But one has to keep in mind that the bias is increased using TSM.

TSM and HPE

The truncated solver method can also be combined with the hopping parameter expansion. Therefore the inverse of the Klein-Gordon operator calculated with TSM is used as a starting point for the hopping parameter expansion. For all different combinations of parameters for the TSM that had been used before, the propagator was calculated with $k = 0, 2, 4, 6$ and 10 terms in the HPE. In addition the CPU time was measured for each calculation. Again one can look at the variance of the (0,0)-component of the propagator times the CPU time. For $N_1 = 950$ the obtained values are shown in figure 4.9. For the other N_1 the plots look quite similar.

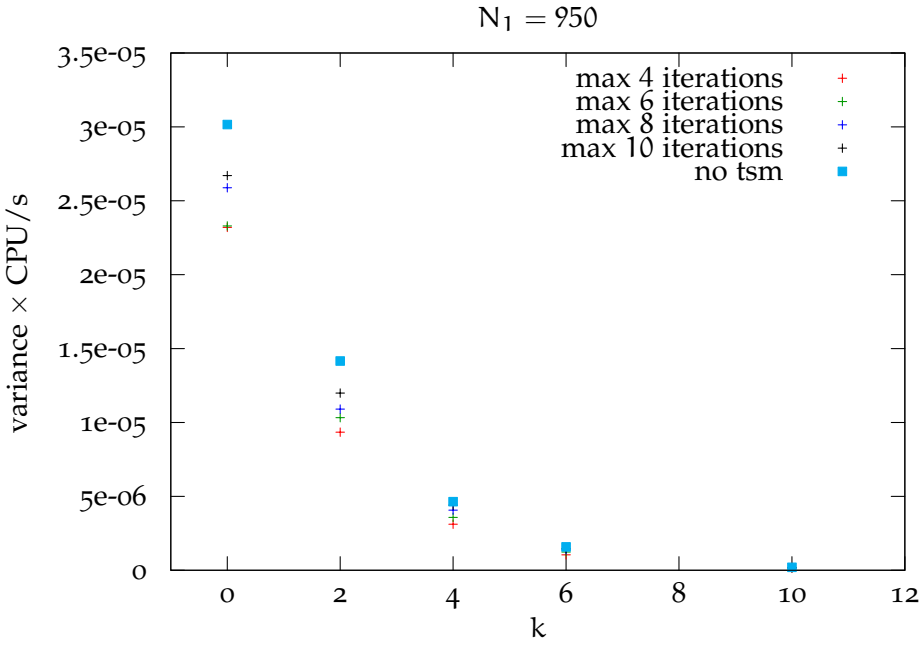

Figure 4.9: TSM and HPE: variance of the (0,0) component of the propagator times CPU time used

If no hopping parameter expansion is done or only few terms are used, the values for TSM are clearly lower than the ones without. But one can also see, that the effect of taking more terms in the HPE is bigger than the effect of the TSM. If enough terms in the hopping parameter expansion are used the effect of the truncated solver method is negligible.

5

THE WILSON-DIRAC OPERATOR

In the last section we have seen that the hopping parameter expansion is the best of the tested methods to improve the calculation of the propagator from a lattice point to itself. The HPE reduces the errors of the diagonal entries of the propagator, while the required computer time is negligible compared to the time needed for the inversion. Since, as the Klein-Gordon operator, the Wilson-Dirac operator connects every lattice point only with itself and with the immediate neighbours, the effects of the three tested methods should be similar when applying them to the Wilson-Dirac operator. Therefore in the following we will focus on using the HPE.

5.1 THE UNIMPROVED WILSON-DIRAC OPERATOR

To calculate a quark propagator, the Dirac operator on the lattice has to be inverted. This can be done using stochastic sources. Since the hopping parameter expansion is easier in this case, at first the unimproved Wilson-Dirac operator (2.31)

$$\begin{aligned} D_W(n|m) &= \left(\frac{4}{a} + m\right)\delta_{m,n} \\ &- \frac{1}{2a}\sum_{\mu=0}^{3}\left(U_\mu(n)(1-\gamma_\mu)\delta_{n+a\mu,m} + U_{-\mu}(n)(1+\gamma_\mu)\delta_{n-a\mu,m}\right) \end{aligned} \tag{5.1}$$

will be looked at. For this a 4-dimensional 8×8^3 lattice with nearly free quarks, i.e. the $SU(3)$ gauge fields $U_\mu(n)$ are close to the unit matrix for every lattice point, was used. For the quarks isospin symmetry is assumed, so $m_u = m_d$. As hopping parameter $\kappa = 0.1$ was chosen. For the random sources $U(1)$ sources were used. Thus one has an entry $\exp(iz)$ with a random number $0 \leqslant z < 2\pi$ for every lattice point, Dirac- and colour-component of $|\eta\rangle$. These sources fulfil the required properties (3.3a) and (3.3b). As a starting point for the calculation of the propagator the DD-HMC (domain decomposed Hybrid Monte Carlo [38]) code[1] by Martin Lüscher was used. Here the Dirac equation

$$D|s\rangle = |\eta\rangle \tag{5.2}$$

is solved using a SAP-GCR (Schwarz preconditioned Generalised Conjugate Residual) solver. A detailed description of the algorithm can be found in [31, 39]. The general idea of the Schwarz procedure is to decompose the lattice in rectangular blocks of equal size and solve the Dirac equation block by block. The Schwarz procedure is used as a preconditioner for the Generalised Conjugate Residual method where the residuals $|\rho\rangle_k = |\eta\rangle - D|s\rangle_k$ with the solution $|s\rangle_k$ after k solver iterations are minimised.

1 The code can be downloaded from http://luscher.web.cern.ch/luscher/DD-HMC/index.html

Implementation of the Hopping Parameter Expansion

A lattice point is called even when the sum of its coordinates $n_0 + n_1 + n_2 + n_3$ is even and odd when this sum is odd. Now one can label the lattice points such that all even points come first and then all odd points. By doing this, the Dirac matrix can be split into four blocks

$$Q = \gamma_5 D = \begin{pmatrix} \tilde{Q}_{ee} & \tilde{Q}_{eo} \\ \tilde{Q}_{oe} & \tilde{Q}_{oo} \end{pmatrix}, \tag{5.3}$$

where Q is the hermitian Dirac operator. $\tilde{Q}_{ee}$ ($\tilde{Q}_{oo}$) contains all entries that couple an even (odd) point with an even (odd) point. Since two neighbouring points cannot both be even or both odd, $\tilde{Q}_{ee}$ and $\tilde{Q}_{oo}$ are diagonal in space-time. $\tilde{Q}_{eo}$ and $\tilde{Q}_{oe}$ then contain all entries that couple two neighbours.

With

$$D = \frac{1}{2\kappa}\mathbb{1} - \frac{1}{2}H = \gamma_5 Q \tag{5.4}$$

for the hopping matrix H one obtains

$$H = -2\left(\gamma_5 Q_{eo} + \gamma_5 Q_{oe}\right) \tag{5.5}$$

with

$$Q_{eo} \equiv \begin{pmatrix} 0 & \tilde{Q}_{eo} \\ 0 & 0 \end{pmatrix} \qquad \text{etc.} \tag{5.6}$$

For the powers of the hopping matrix one obtains

$$\begin{aligned} H^k &= (-2)^k \left(\gamma_5 Q_{eo} + \gamma_5 Q_{oe}\right)^k \\ &= (-2)^k (\underbrace{\cdots \gamma_5 Q_{eo} \cdot \gamma_5 Q_{oe}}_{k \text{ factors}} + \underbrace{\cdots \gamma_5 Q_{oe} \cdot \gamma_5 Q_{eo}}_{k \text{ factors}}) . \end{aligned} \tag{5.7}$$

In (5.7) one makes use of

$$\begin{aligned} \gamma_5 Q_{eo} \cdot \gamma_5 Q_{eo} &= \begin{pmatrix} 0 & \gamma_5 \tilde{Q}_{eo} \\ 0 & 0 \end{pmatrix} \cdot \begin{pmatrix} 0 & \gamma_5 \tilde{Q}_{eo} \\ 0 & 0 \end{pmatrix} = 0 \\ \gamma_5 Q_{oe} \cdot \gamma_5 Q_{oe} &= 0 . \end{aligned} \tag{5.8}$$

To make the calculation of the hopping parameter expansion as easy as possible one should use a maximum number of 8 terms for $\Gamma = \{\gamma_5, \gamma_\mu \gamma_5\}$ and 4 terms otherwise as explained in section 3.4. Then only

$$D^{-1} = (\kappa H)^k \cdot \frac{1}{N} \sum_{i=1}^{N} |s^i\rangle\langle\eta^i| \tag{5.9}$$

has to be considered. Taking the trace $\mathrm{Tr}\left(\Gamma \cdot D^{-1}\right)$ and inserting (5.7) one obtains

$$\begin{aligned} &\mathrm{Tr}\left(\Gamma \cdot D^{-1}\right) \\ &= \mathrm{Tr}\left(\Gamma(-2\kappa)^k (\cdots \gamma_5 Q_{eo} \gamma_5 Q_{oe} + \cdots \gamma_5 Q_{eo}) \frac{1}{N} \sum_{i=1}^{N} |s^i\rangle\langle\eta^i|\right) \\ &= (-2\kappa)^k \frac{1}{N} \sum_{i=1}^{N} \langle\eta^i| \Gamma \left(\cdots \gamma_5 Q_{eo} \gamma_5 Q_{oe} + \cdots \gamma_5 Q_{eo}\right) |s^i\rangle . \end{aligned} \tag{5.10}$$

In the last step the cyclicity and the linearity of the trace were used. This can now be used to implement the HPE in the DD-HMC code:

1. Solve the Dirac equation $D|s\rangle = |\eta\rangle$ with a stochastic source $|\eta\rangle$.
2. Apply $\gamma_5 Q_{eo}$ and $\gamma_5 Q_{oe}$ on $|s\rangle$ in turns until k factors have been applied. Here two terms have to be calculated, one starting with $\gamma_5 Q_{eo}$ and one starting with $\gamma_5 Q_{oe}$. These two terms have to be summed.

$$\underbrace{\cdots \gamma_5 Q_{eo} \cdot \gamma_5 Q_{oe}}_{k \text{ factors}} |s\rangle + \underbrace{\cdots \gamma_5 Q_{oe} \cdot \gamma_5 Q_{eo}}_{k \text{ factors}} |s\rangle$$

3. Apply the Dirac matrix Γ.
4. Calculate the scalar product with the source $\langle\eta|$.
5. Repeat 1. to 4. N times with N different random sources and sum the results up. Divide by N and multiply with $(-2\kappa)^k$.

The result in the end is a stochastic estimate for $\mathrm{Tr}\left(\Gamma \cdot D^{-1}\right)$ with N stochastic sources and k terms in the hopping expansion.
For all tests in this chapter only one gauge configuration is used. Thus in the following only statistical means and no gauge means are calculated.

Testing the Hopping Parameter Expansion - pseudoscalar case

To test the hopping parameter expansion for the case of the unimproved Wilson-Dirac operator, the pseudoscalar case was chosen, thus $\Gamma = \gamma_5$ and $\mathrm{Tr}\left(\gamma_5 \cdot D^{-1}\right)$ was calculated. This was done for different numbers of random sources $N = \{5, 10, 20, 30, 50, 100, 200\}$ and different numbers of terms for the hopping parameter expansion $k = \{0, 2, 4, 6, 8\}$. The calculation was performed 12 times with different seeds for the random number generator, whereas the same seeds for every combination of the parameters was used. With the values from the 12 seeds the mean and the standard deviation σ for the real part of the traces were calculated. All obtained means are approximately 0 and in most cases smaller than the standard deviations, thus in agreement with a vanishing pseudoscalar loop. The standard deviation σ one expects to be proportional to $1/\sqrt{N}$. In figure 5.1 the standard deviations are plotted against $1/\sqrt{N}$ for the different values of k. Additionally a function $f(x) = a \cdot x$ was fitted to the data with gnuplot [40] to show the proportionality.

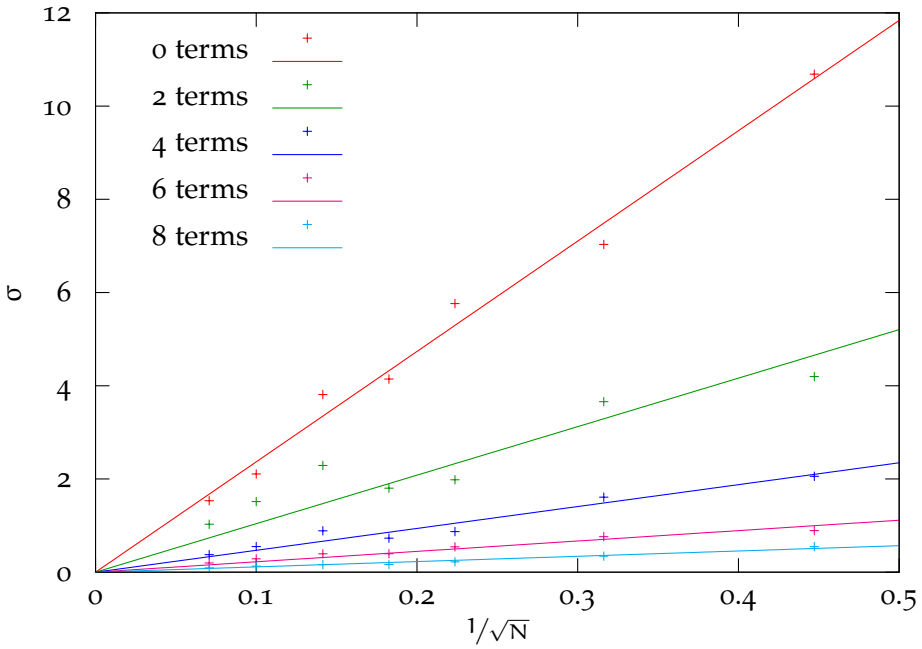

Figure 5.1: Standard deviation after 12 seeds of $\mathrm{Re}\left[\mathrm{Tr}\left(\gamma_5 \cdot D^{-1}\right)\right]$ calculated with hopping parameter expansion without clover term

It is obvious that also for the Wilson-Dirac operator the calculation of the propagator is improved when the hopping parameter expansion is applied. The standard deviation gets smaller if more terms are considered. For 8 terms, σ is more than a factor 10 smaller then for 0 terms.

Testing the Hopping Parameter Expansion - scalar case

As a next step one can test if it depends on the choice of Γ how much the hopping expansion improves the calculation. Therefore $\Gamma = \mathbb{1}$ was tested with the same 8×8^3 lattice as before. For the calculation $k = \{0, 2, 4\}$ terms were used in the HPE. If $k > 0$ additionally the first term in the hopping parameter expansion has to be calculated which is trivial (see section 3.4).

$$\mathrm{Tr}\left(\mathbb{1} \cdot D^{-1}\right) = 2\kappa \underbrace{\mathrm{Tr}\left(\mathbb{1}\right)}_{=12\times 8^4} + \kappa^k \mathrm{Tr}\left(H^k D^{-1}\right) \qquad 0 < k \leqslant 4 \tag{5.11}$$

As for the pseudoscalar case $N = \{5, 10, 20, 30, 50, 100, 200\}$ random sources were used. Every calculation was performed 12 times with different seeds for the random number generator and the mean and the standard deviation of $\mathrm{Re}\left[\mathrm{Tr}\left(\mathbb{1} \cdot D^{-1}\right)\right]$ were calculated. For the mean one gets values of the order of the volume of the lattice, so the scalar loop does not vanish. This is expected since the gauge mean of the scalar loop would be the quark condensate on the lattice. In figure 5.2 the standard deviations are plotted against $1/\sqrt{N}$.

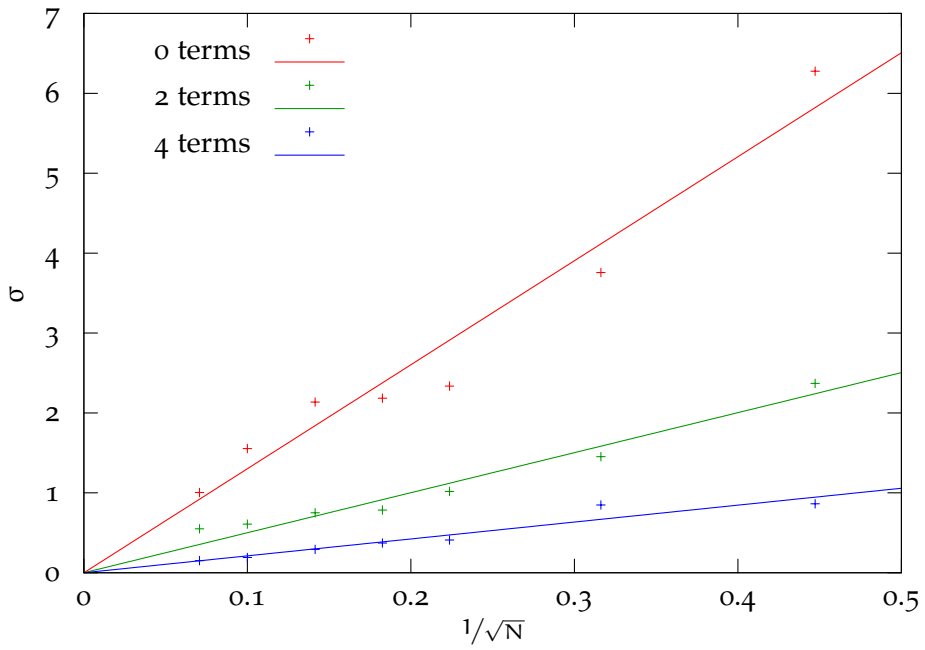

Figure 5.2: Standard deviation after 12 seeds of $\mathrm{Re}\left[\mathrm{Tr}\left(\mathbb{1} \cdot D^{-1}\right)\right]$ calculated with hopping parameter expansion without clover term

Also for the scalar case the calculation of the trace is improved if more terms of the hopping parameter expansion are calculated. The effect of the hopping expansion seems to be independent of the choice of Γ.
In addition one can see that like in the pseudoscalar case σ is proportional to $1/\sqrt{N}$ which is shown by the linear fits.

Testing of Spin Dilution

With the Dirac operator also spin dilution can be tested. Here the random sources have only non-vanishing entries for one Dirac component. For the test the pseudoscalar case $\mathrm{Tr}\left(\gamma_5 \cdot D^{-1}\right)$ was used. To obtain about the same numbers of sources as for the calculation without spin dilution, $N_s = \{1, 3, 5, 7, 12, 25, 50\}$ sources for every Dirac component were used. This are in total $N = \{4, 12, 20, 28, 48, 100, 200\}$ random sources. Again the calculation was performed 12 times with different seeds and the standard deviation σ was calculated. In figure 5.3 the standard deviations are shown for the calculation with spin dilution and for the calculation without spin dilution. For these values no hopping parameter expansion was performed.

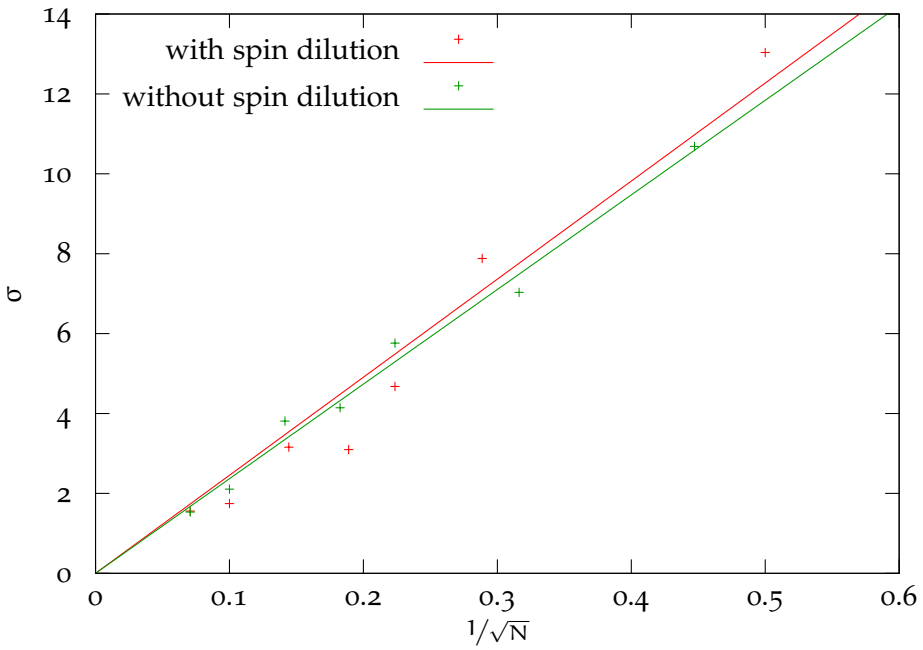

Figure 5.3: Standard deviation after 12 seeds of $\mathrm{Re}\left[\mathrm{Tr}\left(\gamma_5 \cdot D^{-1}\right)\right]$ calculated with and without spin dilution

As one can see for the standard deviation of $\mathrm{Re}\left[\mathrm{Tr}\left(\gamma_5 \cdot D^{-1}\right)\right]$ it makes no difference if spin dilution is used in the calculation.

5.2 THE WILSON-DIRAC OPERATOR WITH CLOVER TERM

For the $\mathcal{O}(a)$-improved Wilson-Dirac operator the hopping parameter expansion has to be adapted as described in section 3.4. The propagator then can be calculated according to (3.25).

$$D_{sw}^{-1} = \sum_{i=0}^{k-1} \left(\frac{1}{2} A^{-1} H\right)^i A^{-1} + \left(\frac{1}{2} A^{-1} H\right)^k \cdot \frac{1}{N} \sum_{i=1}^{N} |s^i\rangle\langle\eta^i| \tag{5.12}$$

Implementation of the hopping parameter expansion for the $\mathcal{O}(a)$-improved Wilson-Dirac operator

As already mentioned in the case of the $\mathcal{O}(a)$-improved Wilson-Dirac operator additionally the matrix

$$A = \left(m + \frac{4}{a}\right) + c_{sw} a \frac{i}{4} \sigma_{\mu\nu} \hat{F}_{\mu\nu} \tag{5.13}$$

has to be inverted. In section 3.4 it was shown that this requires the inversion of two 6×6 matrices for every lattice point. In the DD-HMC code this is done by Householder triangularisation [35].

The first part of the hopping parameter expansion

$$\sum_{i=0}^{k-1} \left(\frac{1}{2} A^{-1} H\right)^i A^{-1} \tag{5.14}$$

now also has to be calculated since the traces do not vanish up to some order k. This can also be done stochastically by inserting a unit matrix in (5.14) and calculating it with M stochastic sources $|\theta^i\rangle$ using (3.3b).

$$\frac{1}{M} \sum_{j=1}^{M} |\theta^j\rangle\langle\theta^j| = \mathbb{1} + \mathcal{O}(1/\sqrt{M})$$

For the traces $\mathrm{Tr}\left(\Gamma \cdot D_{sw}^{-1}\right)$ one obtains

$$\begin{aligned} \mathrm{Tr}\left(\Gamma \cdot D_{sw}^{-1}\right) = &\frac{1}{M} \sum_{j=1}^{M} \sum_{i=0}^{k-1} \langle\theta^j| \Gamma \left(\frac{1}{2} A^{-1} H\right)^i A^{-1} |\theta^j\rangle \\ &+ \frac{1}{N} \sum_{i=1}^{N} \langle\eta^i| \Gamma \left(\frac{1}{2} A^{-1} H\right)^k |s^i\rangle . \end{aligned} \tag{5.15}$$

Therefore one has to calculate the powers of $\left(\frac{1}{2} A^{-1} H\right)$. The hopping matrix H can again be replaced by $H = (-2)(\gamma_5 Q_{eo} + \gamma_5 Q_{oe})$. Then one obtains

$$\begin{aligned} \left(\frac{1}{2} A^{-1} H\right)^i &= \left(-A^{-1} (\gamma_5 Q_{eo} + \gamma_5 Q_{oe})\right)^i \\ &= (-1)^i \Big(\underbrace{\cdots A^{-1} \gamma_5 Q_{eo} \cdot A^{-1} \gamma_5 Q_{oe}}_{i \text{ factors}} + \underbrace{\cdots A^{-1} \gamma_5 Q_{oe} \cdot A^{-1} \gamma_5 Q_{eo}}_{i \text{ factors}} \Big). \end{aligned} \tag{5.16}$$

The code for the second term in (5.15)

$$(-1)^k \frac{1}{N} \sum_{i=1}^{N} \langle \eta^i | \Gamma \left(\cdots A^{-1} \gamma_5 Q_{eo} \cdot A^{-1} \gamma_5 Q_{oe} + \cdots A^{-1} \gamma_5 Q_{eo} \right)^k | s^i \rangle \quad (5.17)$$

can in principle stay the same as for the unimproved Dirac-Wilson operator, except that one has to apply A^{-1} after every step where $\gamma_5 Q_{eo}$ or $\gamma_5 Q_{oe}$ has been applied and also the factor $(-2\kappa)^k$ has to be replaced by $(-1)^k$.

For the first term of (5.15)

$$\frac{1}{M} \sum_{j=1}^{M} \sum_{i=0}^{k-1} (-1)^i \langle \theta^j | \Gamma \left(\cdots A^{-1} \gamma_5 Q_{oe} + \cdots A^{-1} \gamma_5 Q_{eo} \right)^i A^{-1} | \theta^j \rangle \quad (5.18)$$

one first has to apply A^{-1} to the source $|\theta^j\rangle$. After this

$$\left(\cdots A^{-1} \gamma_5 Q_{eo} \cdot A^{-1} \gamma_5 Q_{oe} + \cdots A^{-1} \gamma_5 Q_{eo} \right)$$

has to be applied on $A^{-1}|\theta^j\rangle$ which can be done in the same manner as for the other term. Then Γ is multiplied and the scalar product with $\langle \theta^j |$ is performed. Now all scalar products for the different values of i have to be summed up. A sum over M different random sources has to be performed and the result has to be divided by M.

For the standard deviation of the traces, one now has two influences: The part in the hopping expansion where the inverse calculated by N stochastic sources is needed and the other part which is calculated by M stochastic sources. One expects that the variances for these two parts add up, thus for the standard deviation a behaviour

$$\sigma = \sqrt{\frac{a}{N} + \frac{b}{M}} \quad (5.19)$$

is expected. M can be chosen quite large, since no solution of the Dirac equation is required for the M sources, and therefore the calculation is cheap.

The 8×8^3 Lattice

A first test of the hopping parameter expansion with clover term is done with the same 8×8^3 lattice as before. The HPE adapted to the improved Wilson-Dirac operator, should also work for $c_{sw} = 0$. For the matrix A one simply obtains

$$A = \left(m + \frac{4}{a} \right) + c_{sw} a \frac{i}{4} \sigma_{\mu\nu} \hat{F}_{\mu\nu} = \left(m + \frac{4}{a} \right) = \frac{1}{2\kappa}. \quad (5.20)$$

The trace was calculated for the scalar case $\mathrm{Tr}\,(\mathbb{1} \cdot H)$ with $N = \{5, 10, 20, 30, 50, 100\}$ sources for the inversion and $M = \{100, 200, 500\}$ sources for all other terms in the hopping expansion. The HPE was calculated with $k = \{0, 2, 4, 6\}$ terms. This again was done with 12 different random seeds for every combination of the three parameters N, M and k. The same seeds were used for every combination of the three parameters, so that the first estimation of D^{-1} with

stochastic sources is the same for all calculations with the same N, no matter how many terms in the HPE are calculated afterwards. In figure (5.4) the standard deviations are plotted against $1/\sqrt{N}$ for $M = 500$. The plots for $M = 100$ und $M = 200$ can be found in the appendix (A.1,A.2). To show the behaviour (5.19) a function $f(x) = \sqrt{ax^2 + b}$ with $x = 1/\sqrt{N}$ was fitted to the data with hopping parameter expansion. For the data without HPE (0 terms) $f(x) = ax$ was used again since here no additional terms have to be calculated.

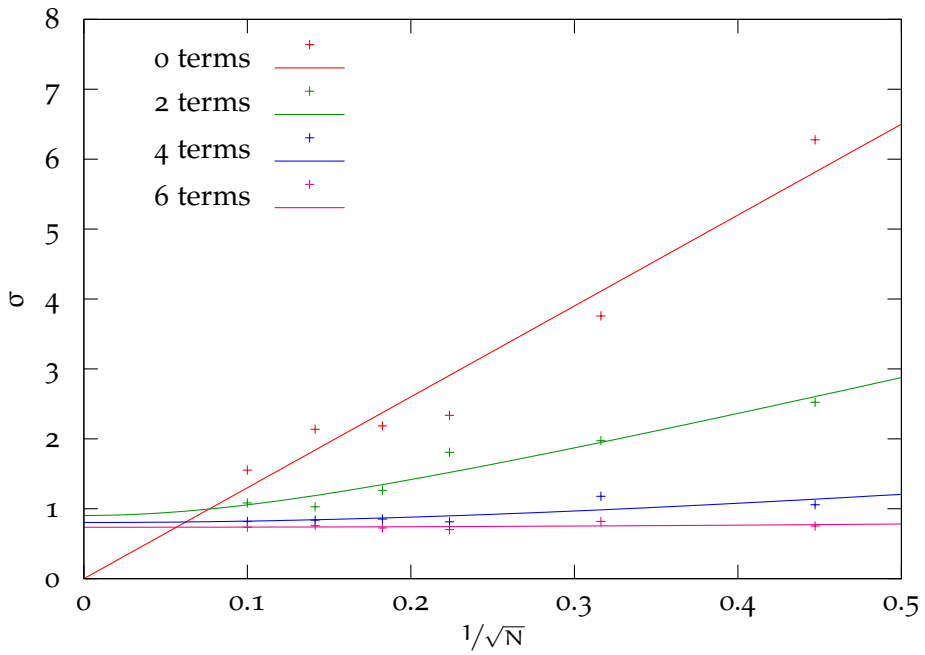

Figure 5.4: Standard deviation after 12 seeds for $\mathrm{Re}\left[\mathrm{Tr}\left(\mathbb{1} \cdot D^{-1}\right)\right]$ of an 8^4 lattice calculated with HPE and $M = 500$ sources for the additional terms

One can clearly see, that the HPE improves the inversion of the Dirac operator even with the additional error of the extra terms that are also calculated stochastically. The standard deviations show the expected dependence on the number of sources N.
If one compares the data for the different values of M, one can see that for bigger M the y-axis intercept decreases a bit as expected. But in the region of interest, namely only few sources for the inversion and therefore high $1/\sqrt{N}$, the influence of the different values of M gets negligible.

CLS configurations

For the following tests and calculations with the $\mathcal{O}(a)$-improved Wilson-Dirac operator we will use configurations from gauge ensembles created as a part of the CLS (Coordinate Lattice Simulations) project [41]. Each CLS ensemble is labelled with a letter and a numeral, for example A5 or E4. Ensembles with the same letter have the same lattice size and the same inverse gauge coupling $\beta = 6/g^2$. Within the ensembles with the same letter an increasing

numeral denotes an increasing value of the hopping parameter κ. In table 5.1 the ensembles we will use are shown with their parameters [42, 43].

Label	lattice	a[fm]	m_π[MeV]	β	κ	c_{sw}
A5	64×32^3	0.082	305.9	5.2	0.13594	2.01715
E2	64×32^3	0.0689	696.5	5.3	0.13590	1.90952
E4	64×32^3	0.0689	554.2	5.3	0.13610	1.90952

Table 5.1: Parameters of the CLS configurations used in this thesis

E4 Lattice

As the first lattice with $c_{sw} \neq 0$ an E4 configuration was used to test the hopping parameter expansion. The E4 lattices have 64×32^3 lattice points. The hopping parameter is $\kappa = 0.13610$, the inverse gauge coupling is $\beta = 5.30$ and $c_{sw} = 1.90952$.
The scalar loop $\mathrm{Tr}\left(\mathbb{1} \cdot D^{-1}\right)$ was calculated for one E4 configuration. For this $N = \{3, 5, 7, 10, 15, 20\}$ sources for the inversion and $M = \{50, 100, 200\}$ sources for the other $k = \{0, 2, 4, 6\}$ terms in the hopping expansion were used. The calculation was repeated with 15 different seeds for the random number generator for all possible combinations of the parameter N, M and k. For $M = 100$ the obtained standard deviations for $\mathrm{Re}\left[\mathrm{Tr}\left(\mathbb{1} \cdot D^{-1}\right)\right]$ are shown in figure 5.5. For the other M the plots can be found in the appendix (A.4,A.6). Again $f(x) = ax$ was fitted to the data with 0 terms and $f(x) = \sqrt{ax^2 + b}$ to the data with HPE, where $x = 1/\sqrt{N}$.

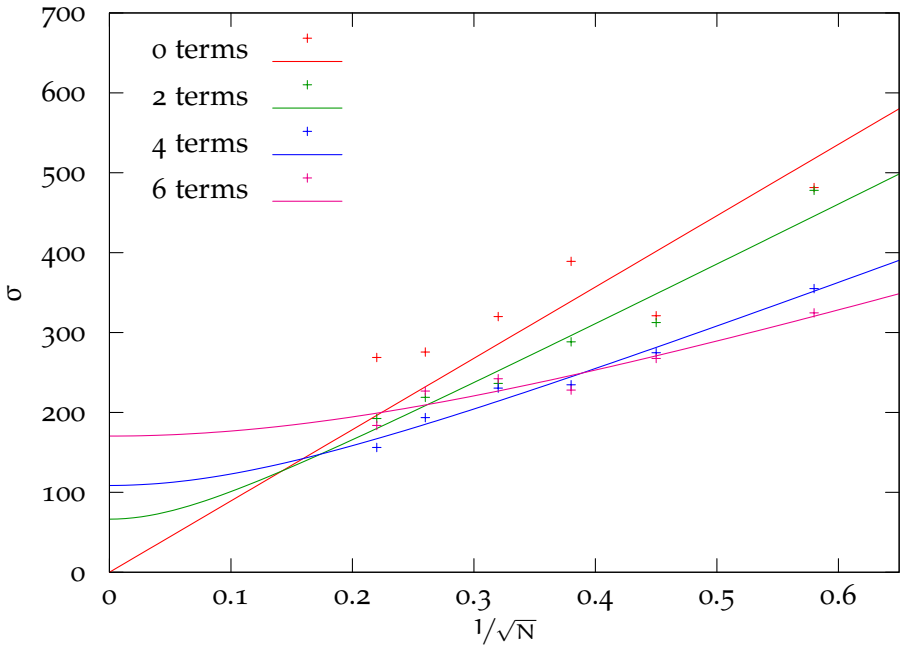

Figure 5.5: Standard deviation after 15 seeds for $\mathrm{Re}\left[\mathrm{Tr}\left(\mathbb{1} \cdot D^{-1}\right)\right]$ of an E4 configuration calculated with HPE and $M = 100$ sources for the additional terms

In the plot one can see that the hopping parameter expansion improves the calculation when just a few sources N are used for the inversion. Since the calculation of D^{-1} with stochastic sources is very expensive in computer time one is interested to minimise the numer of sources N. In the region of interest, i.e. small N, the hopping parameter expansion improves the calculation. In the region of many sources for the stochastic calculation of the propagator, thus small $1/\sqrt{N}$, the hopping parameter expansion worsens the result, because every additional term that is calculated stochastically introduces an additional error. This can be seen in the increasing y-axis intercept for higher k.
As in the case of the 8×8^3 lattice when using more sources M for the additional terms in the HPE the y-axis intercept trends to become smaller. But if only few sources N are used for the inversion, the influence of M is small compared to the influence of the number of terms k in the hopping parameter expansion.
If one compares the effect of the HPE for the E4 lattice and for the 8×8^3 lattice, one can clearly see that the hopping parameter expansion decreases the standard deviation more for the 8×8^3 lattice. This is because of the smaller hopping parameter, which was $\kappa = 0.1$ for the 8×8^3 lattice compared to $\kappa = 0.13610$ in the case of E4. Since the HPE is an expansion in κ, one expects the hopping parameter expansion to better improve the result for smaller κ, thus higher quark masses.

To figure out which set of the parameters is the best, additionally the CPU time needed for every combination of N, M and k was measured. The CPU time turned out to be linear in every parameter except for a slightly larger gap between $k = 0$ and $k = 2$. This is because of the required inversion of $A = \left(m + \frac{4}{a}\right) + c_{sw} a \frac{i}{4} \sigma_{\mu\nu} \hat{F}_{\mu\nu}$ for the hopping parameter expansion. This inversion has to be done only once, no matter how many terms are calculated. Additionally one can see that computing more terms in the HPE is cheap compared to more sources for the inversion. Most of the time needed for the calculation is used for the solution of the sets of linear equations $D|s\rangle = |\eta\rangle$.
In figure 5.6 the variances (standard deviation squared) are plotted against $1/\text{CPUtime}$. Points lying on a vertical line need the same CPU time in the calculation, while the ones that are lowest have the smallest variance for this computational cost.

In the plot one can see that the variance is approximately linear to $1/\text{CPUtime}$. The points marked with arrows are the combinations of parameters M, N and k for which the computational costs seem to be most efficient. These are from left to right $\{N = 7, M = 100, k = 6\}$, $\{N = 7, M = 100, k = 4\}$, $\{N = 7, M = 50, k = 6\}$ and $\{N = 7, M = 50, k = 4\}$.

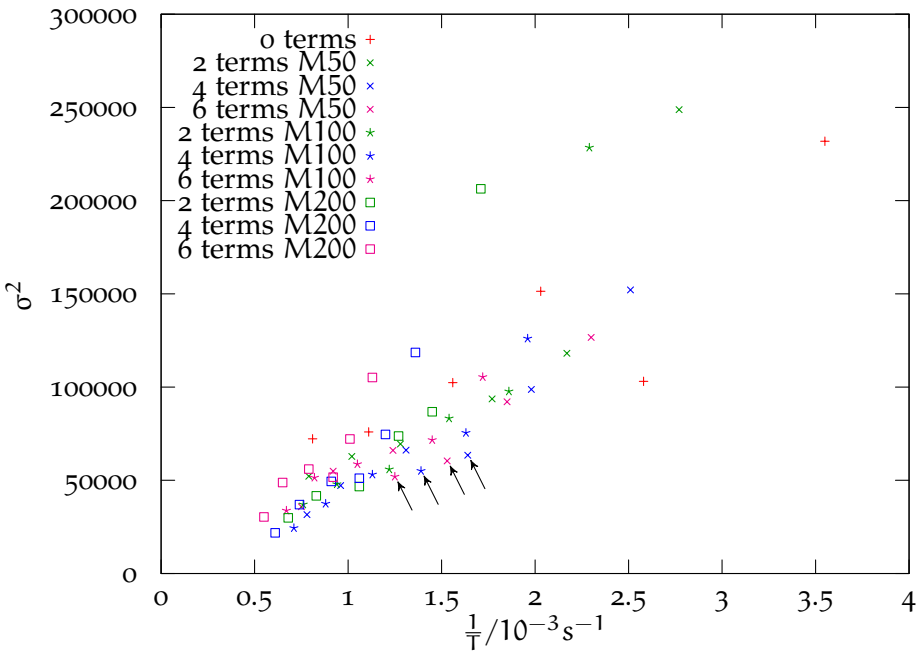

Figure 5.6: Variance after 15 seeds for Re $\left[\mathrm{Tr}\left(\mathbb{1}\cdot D^{-1}\right)\right]$ of an E4 configuration calculated with HPE against $1/\mathrm{CPUtime}$

E2 Lattice

To investigate the dependence of the hopping parameter expansion of the hopping parameter κ, the same as for the E4 lattice was done for an E2 configuration. $\beta = 5.30$ and $c_{SW} = 1.90952$ are the same for E2 and E4. For E2 $\kappa = 0.13590$ is smaller than for E4 ($\kappa_{E4} = 0.13610$).
Again Re $\left[\mathrm{Tr}\left(\mathbb{1}\cdot D^{-1}\right)\right]$ was computed using 15 different seeds for the random number generator. In figure 5.7 the standard deviation is plotted against $1/\sqrt{N}$ for $M = 100$ stochastic sources for the additional terms in the HPE. For $M = 50$ and $M = 200$ the plots can be found in the appendix (A.7,A.9).
One can see that for the E2 lattice the curve for 2 terms in the hopping parameter expansion lies below the other curves. So 2 terms seems to be even better than 4 or 6. This means that for more terms than 2 in the HPE the additional error from the extra terms calculated stochastically is bigger than the gain of the hopping parameter expansion. For this smaller value of κ for the E2 lattice the hopping parameter expansion seems to converge faster.

Additionally the CPU time was measured for every calculation as for the E4 lattice. In figure 5.8 the variance is plotted against $1/\mathrm{CPUtime}$. As expected 2 terms is best, since the standard deviation is the smallest and less terms need less CPU time in the calculation.

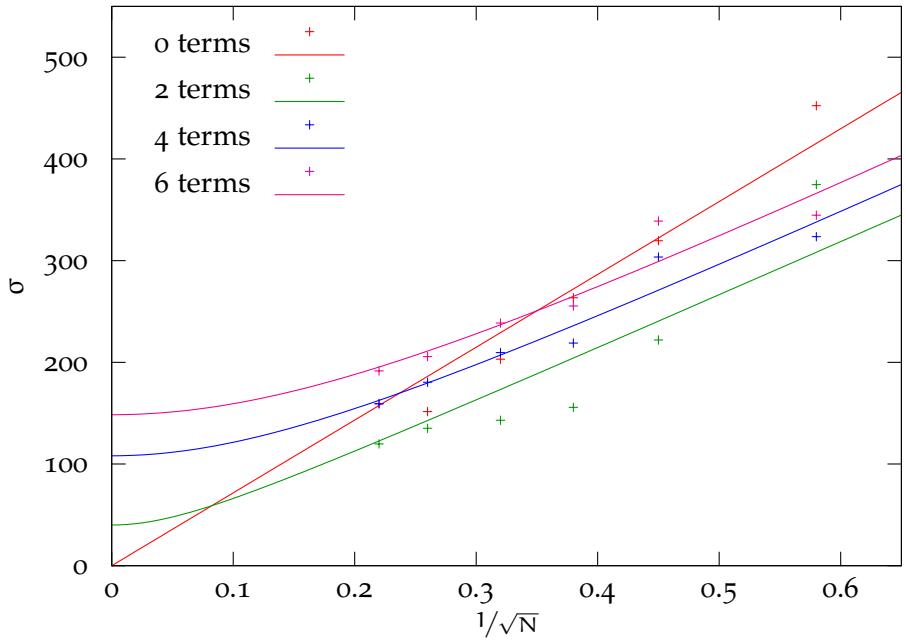

Figure 5.7: Standard deviation after 15 seeds for Re $\left[\mathrm{Tr}\left(\mathbb{1}\cdot D^{-1}\right)\right]$ of an E2 configuration calculated with HPE and $M = 100$ sources for the additional terms

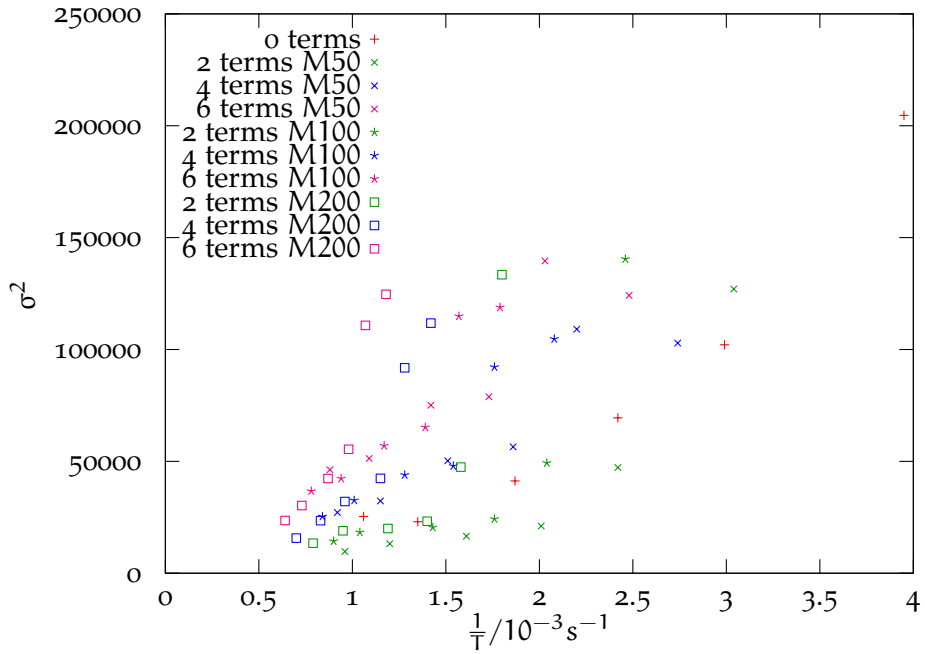

Figure 5.8: Variance after 15 seeds for Re $\left[\mathrm{Tr}\left(\mathbb{1}\cdot D^{-1}\right)\right]$ of an E2 configuration calculated with HPE against $1/\mathrm{CPUtime}$

A5 Lattice

To obtain more information on the dependence of the HPE on the value of κ, the calculation was repeated for an A5 configuration. Here $\kappa = 0.13594$ is in between the values for E2 and E4. The other parameters of the A5 lattice are $\beta = 5.2$ and $c_{sw} = 2.01715$.
In figure 5.9 the standard deviations of $\mathrm{Re}\left[\mathrm{Tr}\left(\mathbb{1} \cdot D^{-1}\right)\right]$ after 15 different seeds are plotted for $M = 100$ random sources for the additional terms. Again for $M = 50$ and $M = 200$ the plots can be found in the appendix (A.10,A.12).

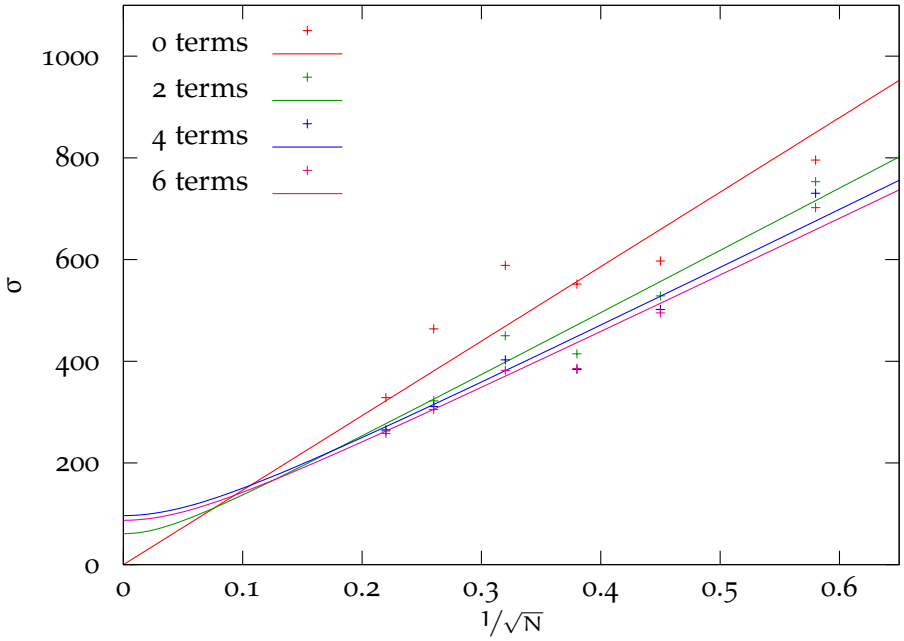

Figure 5.9: Standard deviation after 15 seeds for $\mathrm{Re}\left[\mathrm{Tr}\left(\mathbb{1} \cdot D^{-1}\right)\right]$ of an A5 configuration calculated with HPE and $M = 100$ sources for the additional terms

On can see that for the A5 lattice the hopping parameter expansion improves the calculation most from 0 to 2 terms. From 2 to 4 terms the standard deviations get a bit smaller, but from 4 to 6 terms the standard deviations nearly stay the same.

In figure 5.10 the variances are plotted against $1/\mathrm{CPUtime}$ as done for E4 and E2. The point marked with the arrow seems to be the best one. This is $N = 7$ stochastic sources for the inversion, $k = 4$ terms in the hopping parameter expansion and $M = 50$ sources for the additional terms. If one looks again at the plots of standard deviation against $1/\sqrt{N}$ one can see that for $N = 7$ ($1/\sqrt{N} \approx 0.378$) the values are below the fit curves due to statistical fluctuations. All standard deviations with 7 sources for the inversion are too small, because the same seeds were used for the random number generators for every combination of the parameters. Therefore all values with $N = 7$ start with the same estimation of D^{-1} before HPE is applied. So if the trace of D^{-1} without hopping parameter expansion is too small, also the term in the HPE containing D^{-1} is too small. All points lying in the circle in figure 5.10 belong to calculations with $N = 7$ and therefore should have a slightly higher variance. But also then the value

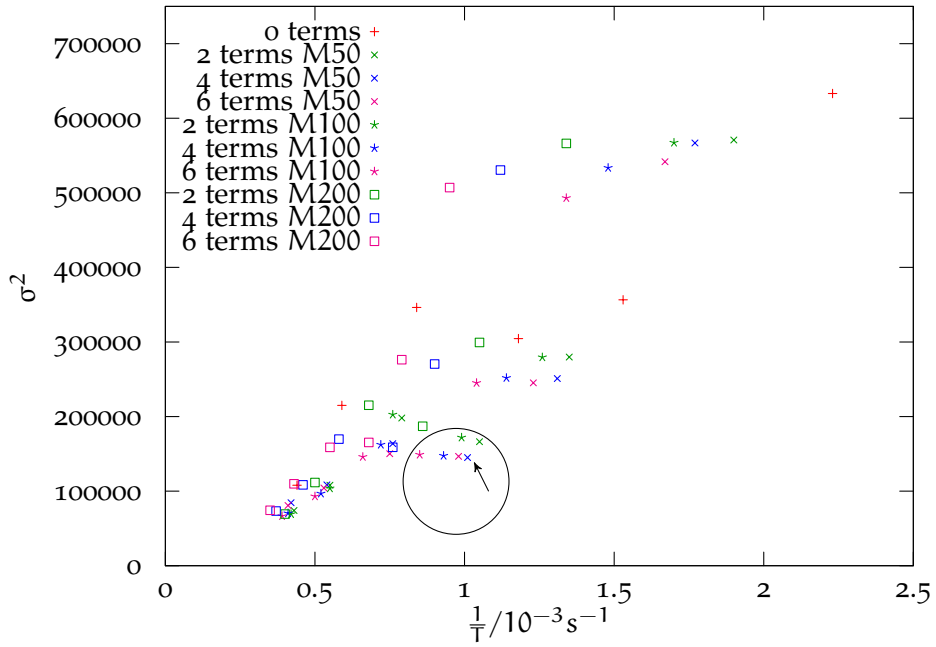

Figure 5.10: Variance after 15 seeds for Re $\left[\mathrm{Tr}\left(\mathbb{1}\cdot D^{-1}\right)\right]$ of an A5 configuration calculated with HPE against $1/\mathrm{CPUtime}$

for $N = 7$, $M = 50$ and $k = 4$ would be one of the best. But to really figure out which combination of parameters is the best, one would need more statistics, which means more different seeds, to remove such statistical fluctuations.

Comparison of E4, E2 and A5

Now one can compare the three different lattices for which $\mathrm{Tr}\left(\mathbb{1} \cdot D^{-1}\right)$ was calculated. For the hopping parameter expansion one expects a different behaviour of convergence for different values of κ. In table 5.2 the values of κ and the pion masses m_π are shown for the three different lattices. In the last row one can find, how many terms k in the hopping parameter expansion it was figured out to be best for the calculation. The columns E2, E4 and A5 are sorted in ascending order of κ.

	E2	A5	E4
κ	0.13590	0.13594	0.13610
m_π[MeV]	696.5	305.9	554.2
HPE	2 terms best	4 terms best	4-6 terms best

Table 5.2: Comparison of E4, E2 and A5

In the table one can see that the number of terms, for which the calculation of the propagator is best, increases with increasing κ. This means for small values of κ the hopping parameter expansion converges faster, as expected. Further dependencies on other lattice parameters could not be observed.
To really confirm the dependency of the convergence of the HPE on the hopping parameter, one would need higher statistics for the lattices already calculated and additional lattices with different values of κ.

The number of sources N can be chosen relatively small for all lattices if HPE is used additionally, for example $N = 7$. Since the inversion with stochastic sources is the most expensive part in CPU time during the calculation, it is favourably that N is as small as possible.
For all lattices one has seen that the number of sources M for the additional terms does not seem to have a big influence on the standard deviations. Therefore $M = 50$ should be sufficient for following calculations.

6

THE PION FORM FACTOR

6.1 HPE AND GAUGE MEAN

For the calculation of observables such as form factors on the lattice, one additionally has to calculate the gauge mean. Taking the gauge mean one obtains two contributions to the variance of the loop, on the one hand the variance due to the gauge fields – the gauge noise – and on the other hand the variance of the stochastic estimate for the propagator. Now one has to check if the reduction of the standard deviations with HPE is also visible after calculating the gauge mean. This is the case if the gauge noise is smaller than the statistical error introduced by the stochastic sources, which can be decreased by the hopping parameter expansion. To obtain the gauge mean, the loop has to be calculated for different gauge configurations of a gauge ensemble. Then the mean of the values for the different configurations has to be taken.
For the form factors one needs the loops at a fixed timeslice, so the traces that are taken are traces over colour-, Dirac- and space-indices. Therefore random sources are used that only have non-vanishing entries for one timeslice as done in time dilution. First of all the scalar loop for 33 different configurations of E4 was calculated for every timeslice. While the number of sources for the additional terms in the HPE was fixed to $M = 50$, the number of terms $k = \{0, 2, 4, 6\}$ in the hopping parameter expansion and the number of sources $N = \{3, 5, 7\}$ for the inversion were varied. For each combination of k and N the gauge mean over the 33 configurations was calculated for every timeslice. In figure 6.1 the obtained standard deviations divided by the means, i.e. the relative errors $\sigma/\langle \text{loop} \rangle$, are plotted against $1/\sqrt{N}$ for the timeslice 0.

Clearly one can see that the hopping parameter expansion improves the calculation of the propagator also in the gauge mean. The y-axis intercept of the linear fit without hopping parameter expansion is the pure gauge noise. The y-axis intercepts gets a bit larger for higher k because of the statistical error from the calculation of the additional terms. One can also see that for 6 terms in the HPE 3 sources for the inversion are sufficient since one gets near the gauge noise and reduction of the standard deviation gets small if more sources are used.

6.2 THE SCALAR CHARGE OF THE PION

As already mentioned in the introduction, in order to calculate the scalar form factor for the charged pion, one has to consider the matrix element [4, 14, 15, 18]

$$\langle \pi^{\pm}(p') | S | \pi^{\pm}(p) \rangle = F_S(Q^2) \qquad \text{with} \qquad S = m_d \bar{d}d + m_u \bar{u}u \,. \tag{6.1}$$

In the following we will concentrate on the scalar charge of the pion, thus the form factor for $Q^2 = -(p' - p)^2 = 0$. Therefore all momenta in (6.1) are set to

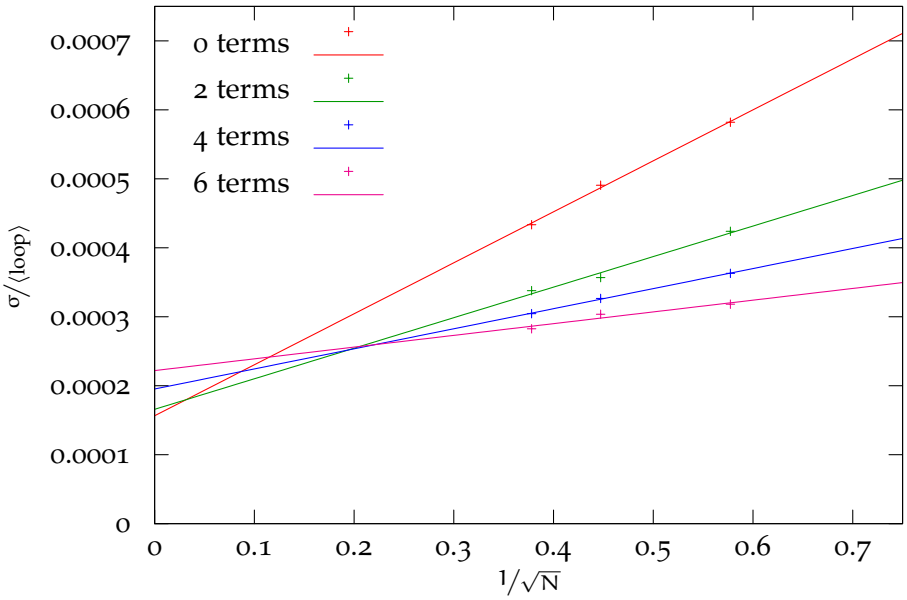

Figure 6.1: Standard deviation divided by gauge mean for the scalar loop at timeslice 0 calculated with stochastic sources and HPE using 33 E4 configurations

zero. For the calculation of the scalar charge one has to calculate three-point functions of the form

$$C_{3pt}(q^2 = 0) = \sum_{\vec{x},\vec{y},\vec{z}} \left\langle \overline{\Psi}(x)_{\alpha,a}(\gamma_5)_{\alpha\beta}\Psi(x)_{\beta,a}\overline{\Psi}(z)_{\gamma,b}\Psi(z)_{\gamma,b}\overline{\Psi}(y)_{\delta,c}(\gamma_5)_{\delta\epsilon}\Psi(y)_{\epsilon,c}\right\rangle . \tag{6.2}$$

Greek letters denote Dirac- and Latin letters colour-indices, respectively. In (6.2) time ordering is assumed, so $x_0 \geqslant z_0 \geqslant y_0$. For simplicity we choose $y_0 = 0$.

As shown in Wick's theorem (2.59) one has to take the sum over all possible contractions. Since only a spinor and an anti-spinor of the same flavour can be contracted only two contractions are possible.

$$\begin{aligned} &\sum_{\vec{x},\vec{y},\vec{z}} \left\langle \overline{\Psi}(x)_{\alpha,a}(\gamma_5)_{\alpha\beta}\Psi(x)_{\beta,a}\overline{\Psi}(z)_{\gamma,b}\Psi(z)_{\gamma,b}\overline{\Psi}(y)_{\delta,c}(\gamma_5)_{\delta\epsilon}\Psi(y)_{\epsilon,c}\right\rangle \\ &+ \sum_{\vec{x},\vec{y},\vec{z}} \left\langle \overline{\Psi}(x)_{\alpha,a}(\gamma_5)_{\alpha\beta}\Psi(x)_{\beta,a}\overline{\Psi}(z)_{\gamma,b}\Psi(z)_{\gamma,b}\overline{\Psi}(y)_{\delta,c}(\gamma_5)_{\delta\epsilon}\Psi(y)_{\epsilon,c}\right\rangle \end{aligned} \tag{6.3}$$

Now the spinors have to be interchanged such, that they are in the right position for the contractions. For the contraction shown below (6.3) this in total produces a minus sign. For the contraction shown above (6.3) one obtains a plus sign. Performing the contractions one finds

$$\begin{aligned} C_{3pt}(0) = &-\sum_{\vec{x},\vec{y},\vec{z}} \left\langle \mathrm{Tr}\{S(\vec{y},0;\vec{x},x_0)\gamma_5 S(\vec{x},x_0;\vec{z},z_0)S(\vec{z},z_0;\vec{y},0)\gamma_5\}\right\rangle_G \\ &+\sum_{\vec{x},\vec{y},\vec{z}} \left\langle \mathrm{Tr}\{S(\vec{y},0;\vec{x},x_0)\gamma_5 S(\vec{x},x_0;\vec{y},0)\gamma_5\}\,\mathrm{Tr}\{S(\vec{z},z_0;\vec{z},z_0)\}\right\rangle_G . \end{aligned} \tag{6.4}$$

with the propagators $S(x,y) = D^{-1}(x,y)$. In (6.4) the traces are taken in colour- and Dirac-space.

The three-point function C_{3pt} consists of two parts. The first term in (6.4) is connected, whereas the second term is quark disconnected. The corresponding diagrams are shown in figure 6.2.

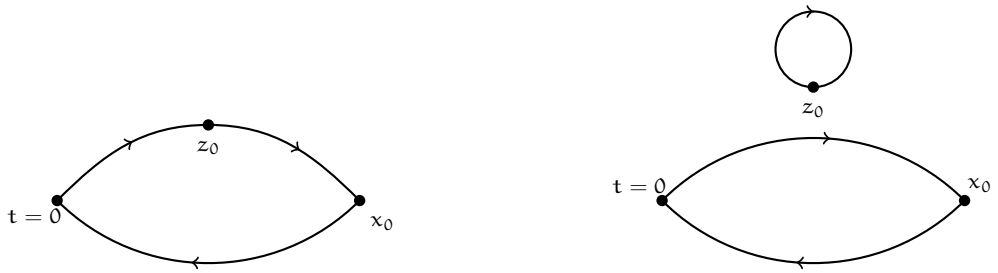

Figure 6.2: The pion three-point function: on the left-hand side the connected part, on the right hand side the quark disconnected part

The three-point function can also be rewritten in terms of creation and annihilation operators of the pion.

$$C_{3pt} = \langle \pi(p')|\mathcal{O}|\pi(p)\rangle = \left\langle \eta_\pi(x_0)\mathcal{O}(z_0)\eta_\pi^\dagger(0)\right\rangle \tag{6.5}$$

with

$$\mathcal{O}(z_0) = \overline{\Psi}(z_0)\Psi(z_0)\,.$$

In (6.5) the momentum and space arguments are supressed. Using the Euclidean time evolution operators one obtains

$$\begin{aligned}
&\left\langle \eta_\pi(x_0)\mathcal{O}(z_0)\eta_\pi^\dagger(0)\right\rangle \\
&= \left\langle \eta_\pi(0)e^{-(x_0-z_0)\hat{H}}\mathcal{O}(0)e^{z_0\hat{H}}\eta_\pi^\dagger(0)e^{-(T-x_0)\hat{H}}\right\rangle \\
&= \sum_i \langle i|\eta_\pi(0)e^{-(x_0-z_0)\hat{H}}\mathcal{O}(0)e^{-z_0\hat{H}}\eta_\pi^\dagger(0)e^{-(T-x_0)\hat{H}}|i\rangle \\
&= \sum_{i,j,k} e^{-(x_0-z_0)E_j}e^{-z_0E_k}e^{-(T-x_0)E_i}\langle i|\eta_\pi(0)|j\rangle\langle j|\mathcal{O}(0)|k\rangle\langle k|\eta_\pi^\dagger(0)|i\rangle\,.
\end{aligned} \tag{6.6}$$

For $0 \ll z_0 \ll x_0 \ll T$ states with high energies are exponentially suppressed. In first order only the state with lowest possible energy contributes to the three-point function. Since $\eta_\pi(0)|0\rangle = \langle 0|\eta_\pi^\dagger(0) = 0$ one obtains

$$\begin{aligned}
C_{3pt} &= e^{-(x_0-z_0)E_\pi}e^{-z_0E_\pi}\langle 0|\eta_\pi(0)|\pi\rangle\langle\pi|\mathcal{O}(0)|\pi\rangle\langle\pi|\eta_\pi^\dagger(0)|0\rangle + \dots \\
&= e^{-x_0m_\pi}\langle 0|\eta_\pi(0)|\pi\rangle\langle\pi|\mathcal{O}(0)|\pi\rangle\langle\pi|\eta_\pi^\dagger(0)|0\rangle + \dots
\end{aligned} \tag{6.7}$$

with $E_\pi = m_\pi$ for $\vec{p} = 0$.

A similar calculation can be done for the two-point function $\langle\pi(p')|\pi(p)\rangle$. Using Wick's theorem one obtains

$$\begin{aligned}
C_{2pt}(q^2 = 0) &= \sum_{\vec{x},\vec{y}}\left\langle \overline{\Psi}(x)\underbrace{_{\alpha,a}(\gamma_5)_{\alpha\beta}\Psi(x)_{\beta,a}\overline{\Psi}(y)}_{\gamma,b}(\gamma_5)_{\gamma\delta}\Psi(y)_{\delta,b}\right\rangle \\
&= -\sum_{\vec{x},\vec{y}}\left\langle \mathrm{Tr}\left\{S(\vec{y},0;\vec{x},x_0)\gamma_5 S(\vec{x},x_0;\vec{y},0)\gamma_5\right\}\right\rangle_G\,.
\end{aligned} \tag{6.8}$$

Again creation and annihilation operators can be used. Inserting time evolution for the two-point function one obtains

$$C_{2pt} = e^{-x_0 m_\pi} \langle 0|\eta_\pi(0)|\pi\rangle \langle \pi|\eta_\pi^\dagger(0)|0\rangle + \dots \tag{6.9}$$

If one takes the ratio of the three-point function (6.7) and the two-point function (6.9) the exponential behaviour of C_{2pt} and C_{3pt} cancels out.

$$R(x_0, z_0) = \frac{C_{2pt}}{C_{3pt}} = \langle \pi(\vec{p} = 0)|\mathcal{O}(0)|\pi(\vec{p} = 0)\rangle = \langle \pi(\vec{p} = 0)|\overline{\Psi}\Psi|\pi(\vec{p} = 0)\rangle \tag{6.10}$$

This is the form factor at $Q^2 = 0$ we are interested in.

To calculate the disconnected contribution to the ratio (6.10) one has to take into account the non-vanishing vacuum expectation value

$$\langle \mathrm{Tr}\{S(\vec{y}, 0; \vec{x}, x_0)\gamma_5 S(\vec{x}, x_0; \vec{y}, 0)\gamma_5\}\rangle_G \langle \mathrm{Tr}\{S(\vec{z}, z_0; \vec{z}, z_0\}\rangle_G , \tag{6.11}$$

which has to be subtracted from the disconnected part of the three-point function. Thus the disconnected contribution R_{disc} to the ratio (6.10) is obtained through

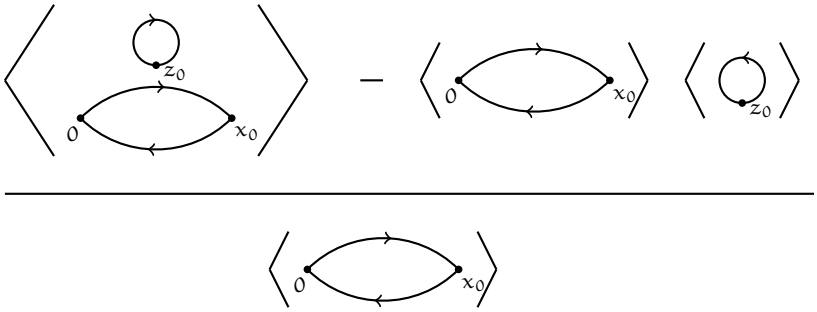

where the brackets stand for taking the gauge mean.

The required loop was calculated for 81 E4 configurations with 3 stochastic sources for the inversion and 50 stochastic sources for the additional 6 terms in the hopping parameter expansion. The two-point functions were already calculated [44].

To extract the disconnected contribution from the data the summation method [10, 45] was used. Here the ratios $R(x_0, z_0)$ are summed for z_0 up to x_0 to reduce the influence of the higher order corrections to (6.10). For the summed ratios one expects that

$$\sum_{z_0=0}^{x_0} R(x_0, z_0) = \langle \pi|\,\overline{\Psi}\Psi\,|\pi\rangle \cdot x_0 \,. \tag{6.12}$$

The summed ratio is calculated up to $x_0 = 31$, i.e. for half of the timeslices of the lattice. The timeslices $x_0 > 31$ would have to be treated differently due to the periodic boundary conditions of the lattice and time ordering.

The errors for the summed ratios were calculated using the jackknife procedure [19]. Using jackknife the value of interest, here the summed ratio, is calculated

once for all measured configurations. Then one configuration is left out. This is done for all configurations. An estimate for the error of the value is obtained through

$$\sigma^2 = \frac{N-1}{N} \sum_{i=1}^{N} (\theta - \theta_i)^2 , \tag{6.13}$$

where θ is calculated using all configurations and for θ_i configuration i is left out. N is the total number of configurations that are used in the calculation.

In figure 6.3 the summed ratios for the scalar case are plotted against the timeslice x_0. Since one expects a linear behaviour, where the ascending slope is the disconnected contribution to the scalar form factor at $Q^2 = 0$, a linear function was fitted to the data. For the fit timeslices 8 to 31 were used. The errors of the fit parameters were calculated using jackknife.

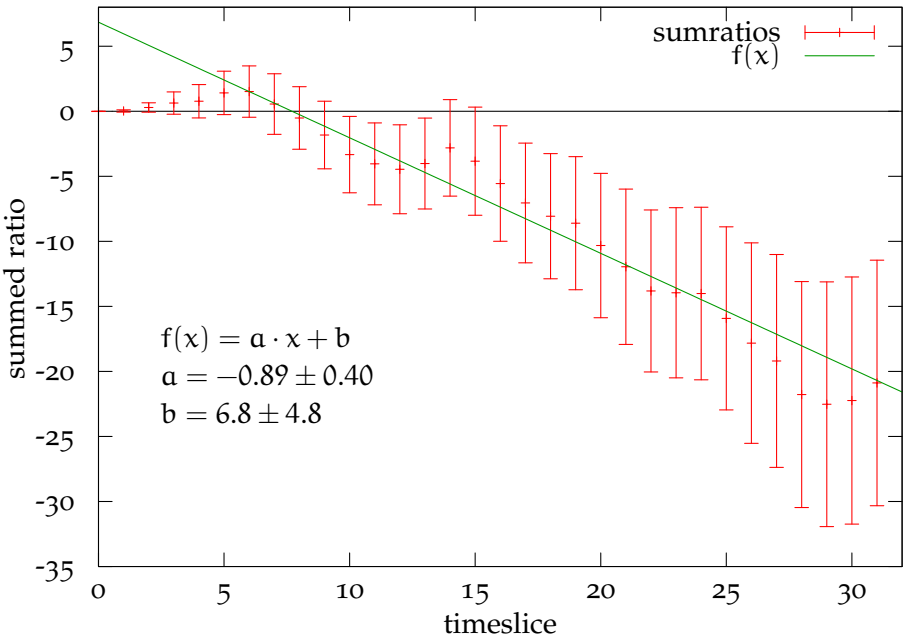

Figure 6.3: Summed ratios for 81 E4 configurations for the disconnected contribution to the scalar charge of the pion

In figure 6.3 one can see the expected linear behaviour of the data, although the errors for the summed ratios are large. When calculating the disconnected contribution one has to subtract two large numbers, the disconnected part of the three point function and the vacuum expectation value. This results in large errors. For the descending slope, which we are interested in, the fit returns

$$a = -0.89 \pm 0.40 . \tag{6.14}$$

Even with the large error the value is more than 2σ away from a vanishing contribution of the disconnected diagram. Of course one should increase the statistics, i.e. calculate more configurations, to reduce the errors of the summed ratios.

Currently it is not possible to compare the disconnected contribution to the connected one, since the connected part of the three-point function has not been measured yet for the scalar case.

6.3 THE VECTOR CHARGE OF THE PION

Additionally the calculation of the ratios described in the previous section was repeated for the vector form factor. The vector form factor is given by [4, 14, 15, 16, 17]

$$\langle \pi(p')|V_\mu|\pi(p)\rangle = (p+p')_\mu F_V(Q^2) \quad \text{with} \quad V_\mu = \frac{2}{3}\bar{u}\gamma_\mu u - \frac{1}{3}\bar{d}\gamma_\mu d\,. \tag{6.15}$$

One can show [7] that in the gauge mean the disconnected loop vanishes in the vector case. Therefore one expects the disconnected contribution to the vector form factor to be zero. In figure 6.4 the summed ratios with $\gamma_\mu = \gamma_0$ for 61 E4 configurations are plotted against the timeslices. Again the errors for the summed ratios were calculated using jackknife.

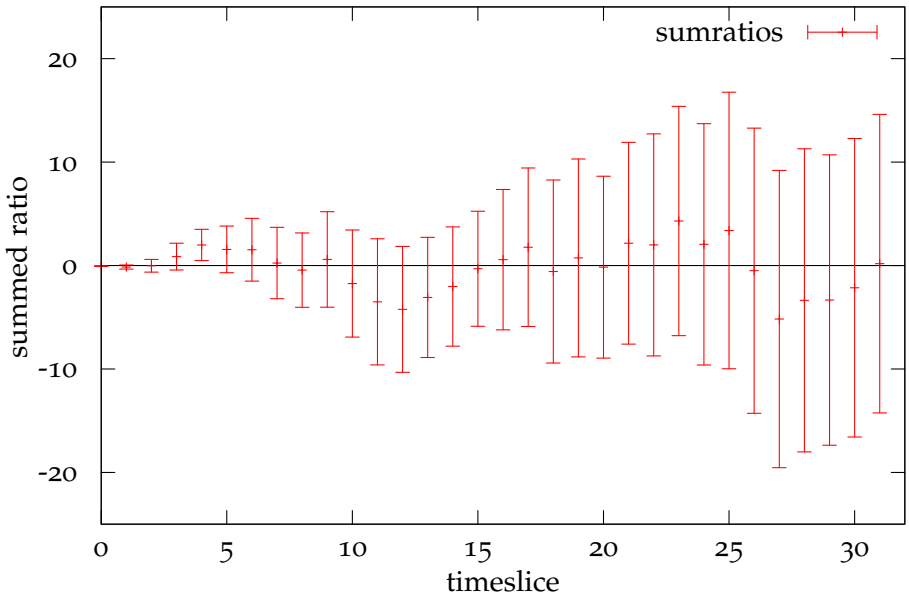

Figure 6.4: Summed ratios for 61 E4 configurations for the disconnected contribution to the vector charge of the pion with γ_0

One can see that this plot is in perfect agreement with a vanishing ascending slope, so a vanishing contribution to the pion vector form factor. If one compares the plots for the disconnected contributions to the scalar form factor 6.3, which is expected to be non-vanishing, and the vector form factor 6.4, which is expected to vanish, one can clearly see a big difference. For the disconnected contribution to the vector form factor no ascending slope can be observed and for the disconnected contribution to the scalar form factor the descending slope is non-zero in a range of 2σ. Thus we have a clear evidence for a non-vanishing contribution to the scalar form factor.

CONCLUSION AND OUTLOOK

The computation of diagrams with quark disconnected loops on the lattice has to be done stochastically, since an explicit calculation with point sources is too expensive in computational costs. Therefore one uses the method of stochastic sources to obtain an estimate for the propagator. Since solving the Dirac equation needs much computer time, one is interested in using as few sources as possible. However, few sources result in larger statistical errors. Thus techniques to improve the stochastic estimates are required. In total three methods - dilution, the hopping parameter expansion and the truncated solver method - have been tested whether they improve the calculation.

Dilution was tested with several dilution schemes. Time dilution turned out to improve the calculation for most entries of the propagator but not for the diagonal ones, which are relevant for the trace and thus for disconnected loops. For even-odd dilution as well as for spin dilution no improvement could be observed in the calculation.
The truncated solver method on the one hand reduces the computer time needed for the calculation, but on the other hand it introduces an additional bias. Thus we decided not to use the TSM for further calculations.
The hopping parameter expansion turned out to improve the stochastic estimates of the quark loops. If the hopping parameter expansion is applied, the statistical error of $\mathrm{Tr}\left(\Gamma \cdot D^{-1}\right)$ decreases without requiring much additional computer time. We were also able to adapt the hopping parameter expansion to the case of the $\mathcal{O}(a)$-improved Wilson-Dirac operator. Even though the additional terms that do not contain the inverse of the Dirac operator also have to be calculated stochastically in this case, a reduction of stochastic errors could be observed when using the HPE. For the lattices we looked at so far (E4, E2 and A5) we figured out that a number of sources N of $\mathcal{O}(1)$ for the inversion is sufficient, if the hopping parameter expansion is used in addition. Also the number of sources for the terms that do not contain the inverse of the Dirac operator can be chosen relatively small, for example $M = 50$. A slight trend was observed that more terms in the HPE are needed for larger values of κ . It seems that the hopping parameter expansion converges faster for smaller κ, thus fewer terms are sufficient. But this trend has to be confirmed with more different lattices and more statistics for a single lattice.

For the E4 lattice the standard deviations in the gauge mean were calculated for various combinations of the number of sources N for the inversion and the number of terms k in the hopping parameter expansion with fixed $M = 50$. When calculating 6 terms in the HPE it turned out that $N = 3$ sources for the inversion are enough, since the reduction of standard deviation gets small when using more sources. For $N = 3$ the standard deviation decreases by a factor of ≈ 2 from 0 to 6 terms. Thus the hopping parameter expansion is an effective tool to improve the stochastic estimate of the disconnected loop. For the calculation

of the form factors we decided to use $N = 3$ sources for the inversion and 6 terms in the HPE.

For the future we have planned to calculate the form factors also on different CLS ensembles, thus different lattice sizes, different hopping parameters κ etc. To perform the calculation of the form factors on other lattices one first has to figure out the best combination of the number of sources N for the inversion, the number of sources M for the additional terms and the order k of the hopping parameter expansion. For this one should start calculating the loop at a single configuration and look at the standard deviations as already done for E4, E2 and A5 in chapter 5. To finally decide which parameters one wants to use for the calculation of the disconnected contribution to the form factor, one has to examine the standard deviations when taking the gauge mean of the loop for different configurations of an ensemble. For E4 this was done in section 6.1.

For in total 81 E4 configurations the disconnected contribution to the scalar charge of the pion was obtained using the ratios of the three-point and the two-point functions and applying the summation method. Here we could confirm in the range of 2σ that the disconnected contribution to the scalar charge of the pion does not vanish. Currently the absolute value

$$a = -0.89 \pm 0.40$$

we obtained cannot be combined with the connected contribution, which has not been calculated for the scalar case yet. Nevertheless, the data have shown how important it is to look at the disconnected contribution to the scalar form factor, since it does not vanish.
For the disconnected contribution to the vector charge, which was calculated on 61 E4 configurations, the obtained data are in complete agreement with a vanishing disconnected contribution as expected. This shows that the applied methods work quite well. But the relative error of the disconnected contribution to the scalar charge still is $0.40/0.89 \approx 45\%$. Thus one needs higher statistics, i.e. more configurations, to further reduce the statistical error of the gauge noise. One also could aim at developing new methods that are even better than the ones used so far.

So far we only have looked at the form factors for momentum transfer $Q^2 = 0$. To investigate the Q^2-dependence of the form factors, the disconnected contributions have to be calculated for different momenta.

The developed methods will also be used for other physical quantities containing disconnected contributions. An example is the strangeness content $\langle N|\bar{s}s|N\rangle$ of the nucleon [5] where these methods can be adapted directly. For some other quantities like the anomalous magnetic moment of the muon [46] the developed methods need further adaptation.

APPENDIX

In the following, some plots for the hopping parameter expansion for the $\mathcal{O}(a)$-improved Wilson-Dirac operator are shown, thus the plots belong to section 5.2. There the trace of the propagator was calculated using 5.15:

$$\operatorname{Tr}\left(\Gamma \cdot D_{sw}^{-1}\right) = \frac{1}{M}\sum_{j=1}^{M}\sum_{i=0}^{k-1}\langle\theta^j|\Gamma\left(\frac{1}{2}\,A^{-1}\,H\right)^i A^{-1}\,|\theta^j\rangle + \frac{1}{N}\sum_{i=1}^{N}\langle\eta^i|\Gamma\left(\frac{1}{2}\,A^{-1}\,H\right)^k|s^i\rangle\,.$$

For the tests of the hopping parameter expansion four different lattices were used (8×8^3, E4, E2 and A5). In all plots the standard deviation is plotted against $1/\sqrt{N}$ each with $k = \{0, 2, 4, 6\}$ terms for the hopping parameter expansion. The data for $k = 0$ is fitted with $f(x) = ax$ and the data for $k > 0$ with $f(x) = \sqrt{ax^2 + b}$, where $x = 1/\sqrt{N}$. For all lattices three plots are shown for three different values of M ($M = \{100, 200, 500\}$ for 8×8^3 and $M = \{50, 100, 200\}$ for E4, E2 and A5).

The 8×8^3 Lattice

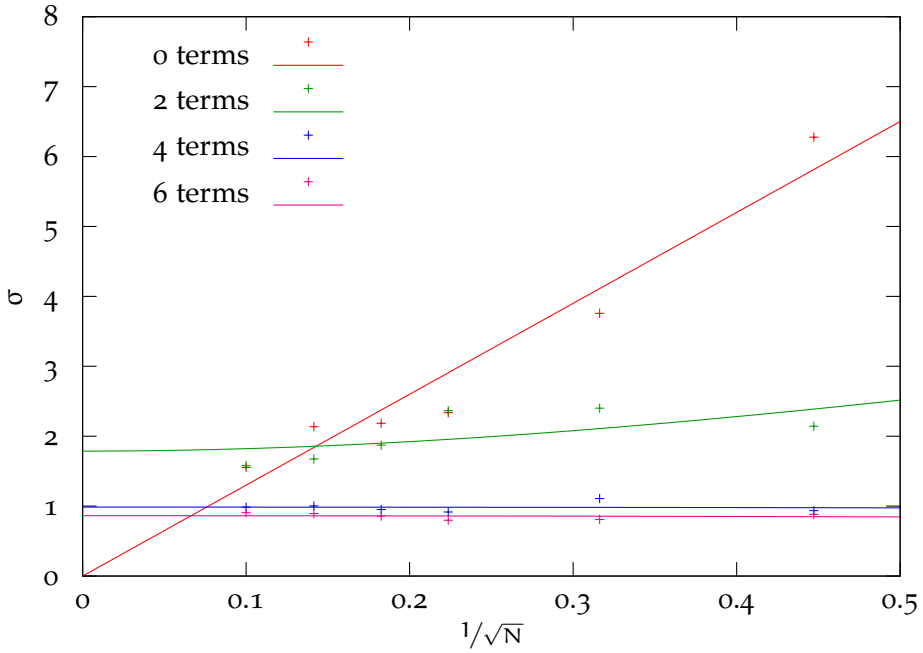

Figure A.1: Standard deviation after 12 seeds for Re $\left[\mathrm{Tr}\left(\mathbb{1} \cdot D^{-1}\right)\right]$ of an 8^4 lattice calculated with HPE and $M = 100$ sources for the additional terms

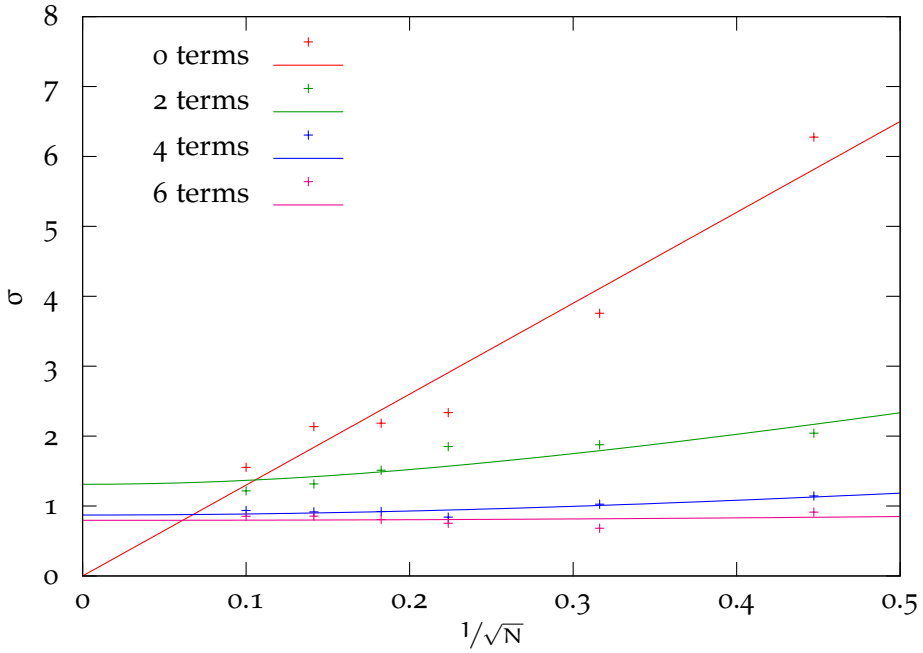

Figure A.2: Standard deviation after 12 seeds for Re $\left[\mathrm{Tr}\left(\mathbb{1} \cdot D^{-1}\right)\right]$ of an 8^4 lattice calculated with HPE and $M = 200$ sources for the additional terms

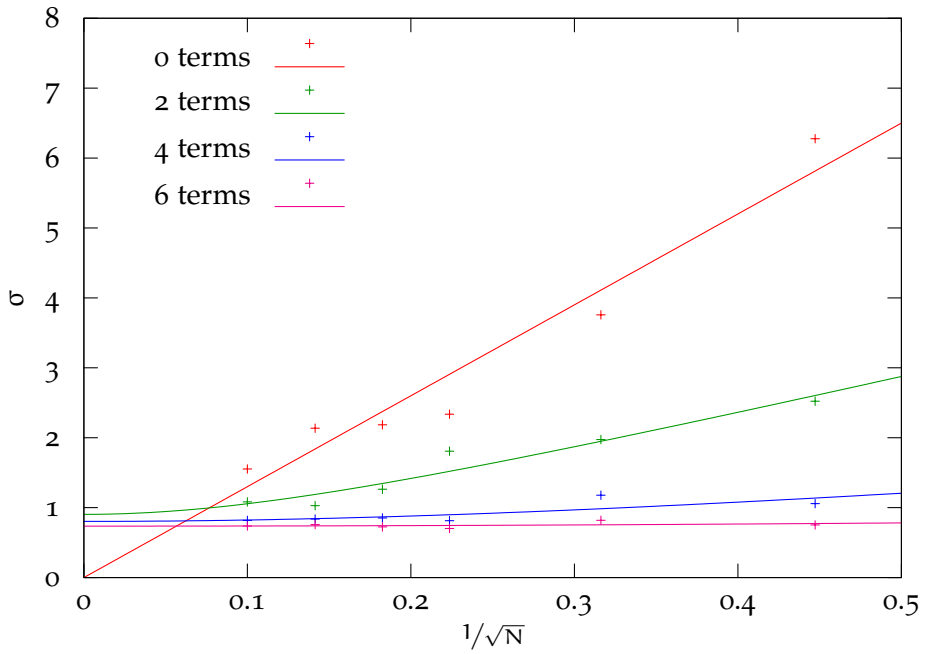

Figure A.3: Standard deviation after 12 seeds for $\mathrm{Re}\left[\mathrm{Tr}\left(\mathbb{1} \cdot D^{-1}\right)\right]$ of an 8^4 lattice calculated with HPE and $M = 500$ sources for the additional terms

The E4 Lattice

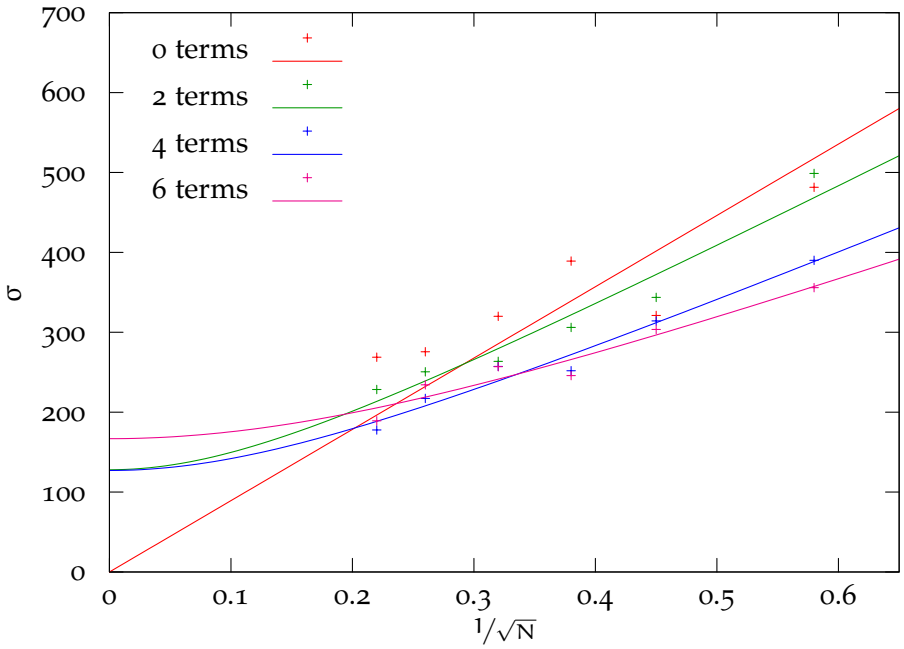

Figure A.4: Standard deviation after 15 seeds for Re $\left[\mathrm{Tr}\left(\mathbb{1}\cdot D^{-1}\right)\right]$ of an E4 configuration calculated with HPE and $M = 50$ sources for the additional terms

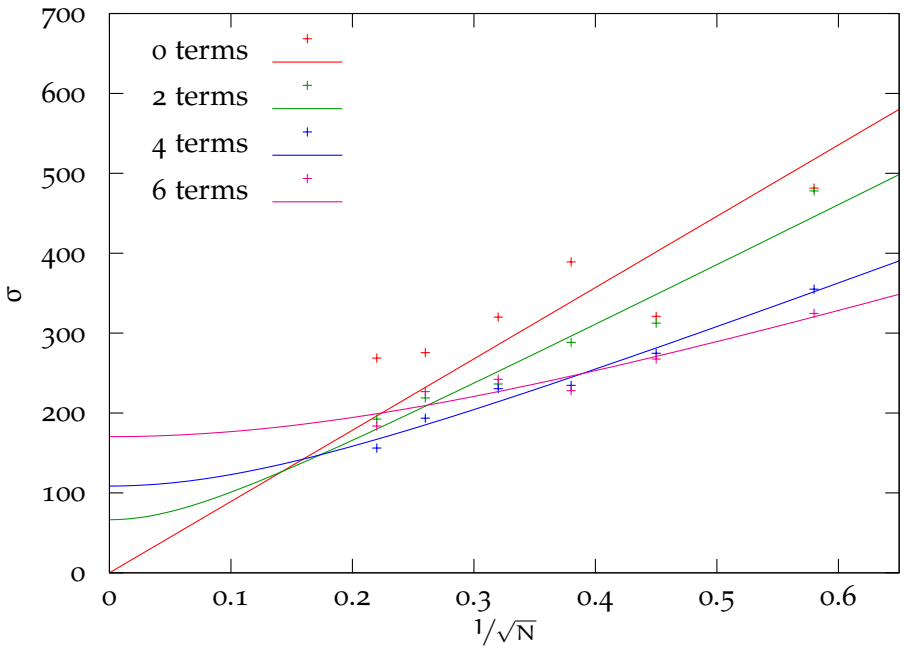

Figure A.5: Standard deviation after 15 seeds for Re $\left[\mathrm{Tr}\left(\mathbb{1}\cdot D^{-1}\right)\right]$ of an E4 configuration calculated with HPE and $M = 100$ sources for the additional terms

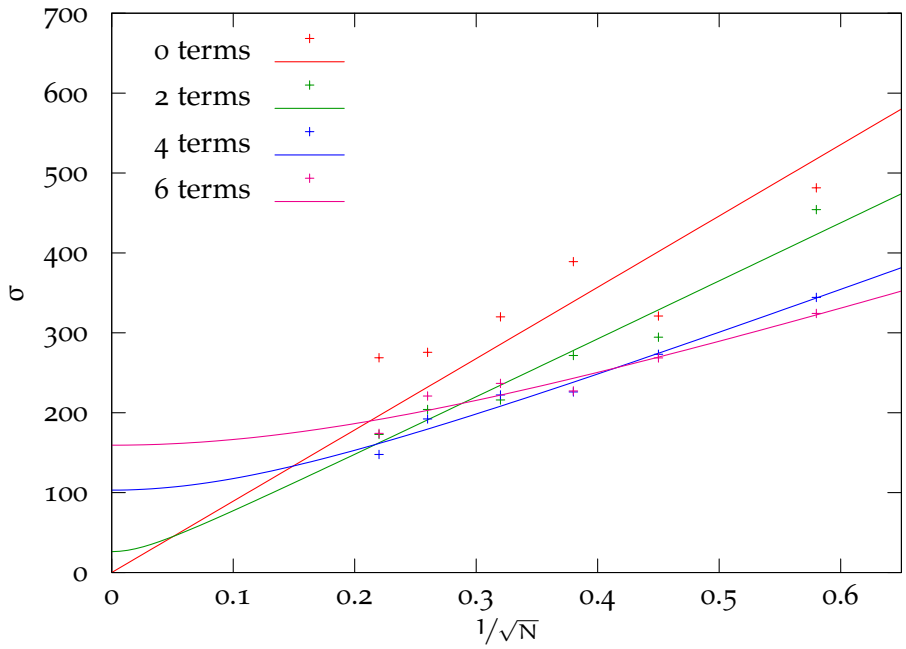

Figure A.6: Standard deviation after 15 seeds for Re $\left[\mathrm{Tr}\left(\mathbb{1} \cdot D^{-1}\right)\right]$ of an E4 configuration calculated with HPE and $M = 200$ sources for the additional terms

The E2 Lattice

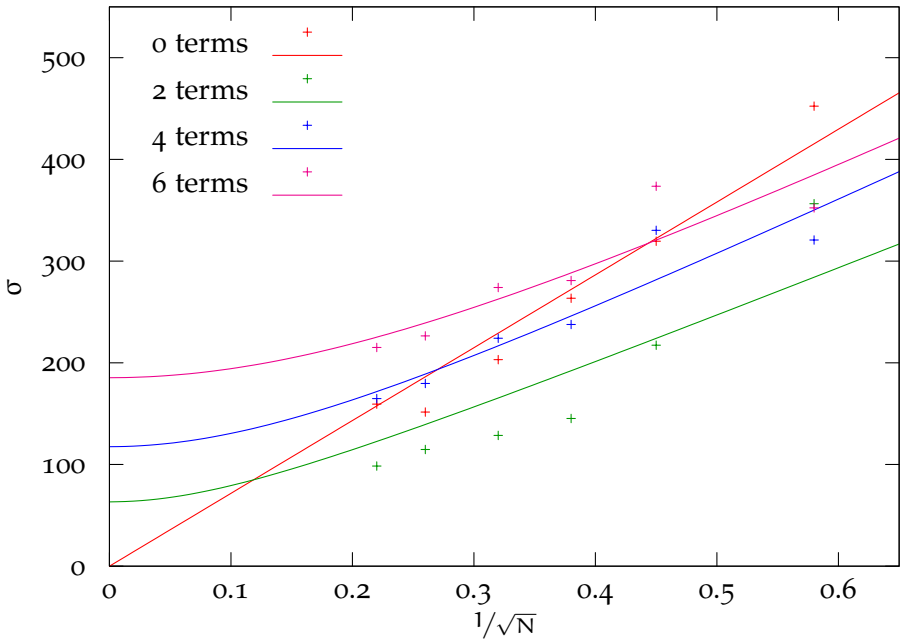

Figure A.7: Standard deviation after 15 seeds for Re $\left[\mathrm{Tr}\left(\mathbb{1} \cdot D^{-1}\right)\right]$ of an E2 configuration calculated with HPE and $M = 50$ sources for the additional terms

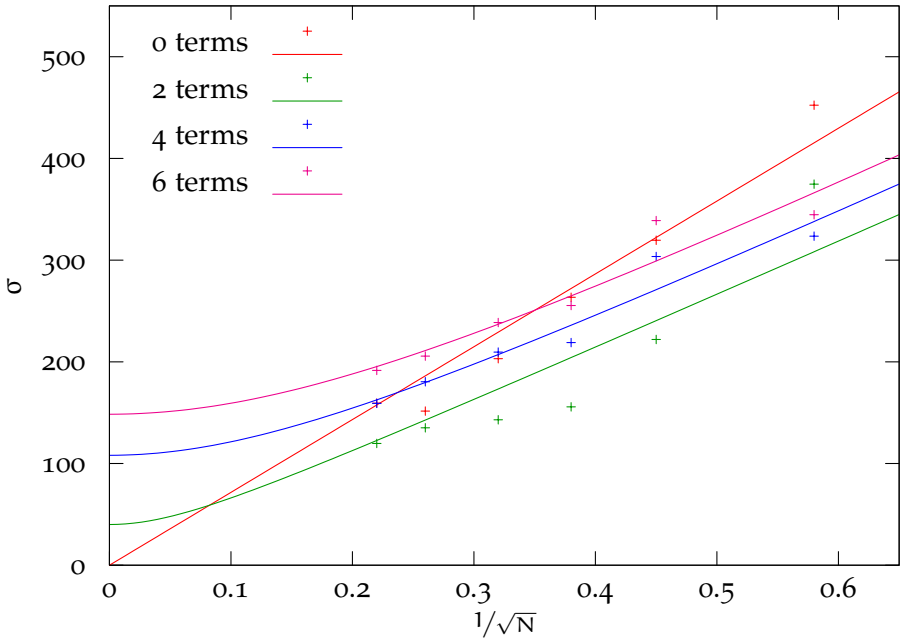

Figure A.8: Standard deviation after 15 seeds for Re $\left[\mathrm{Tr}\left(\mathbb{1} \cdot D^{-1}\right)\right]$ of an E2 configuration calculated with HPE and $M = 100$ sources for the additional terms

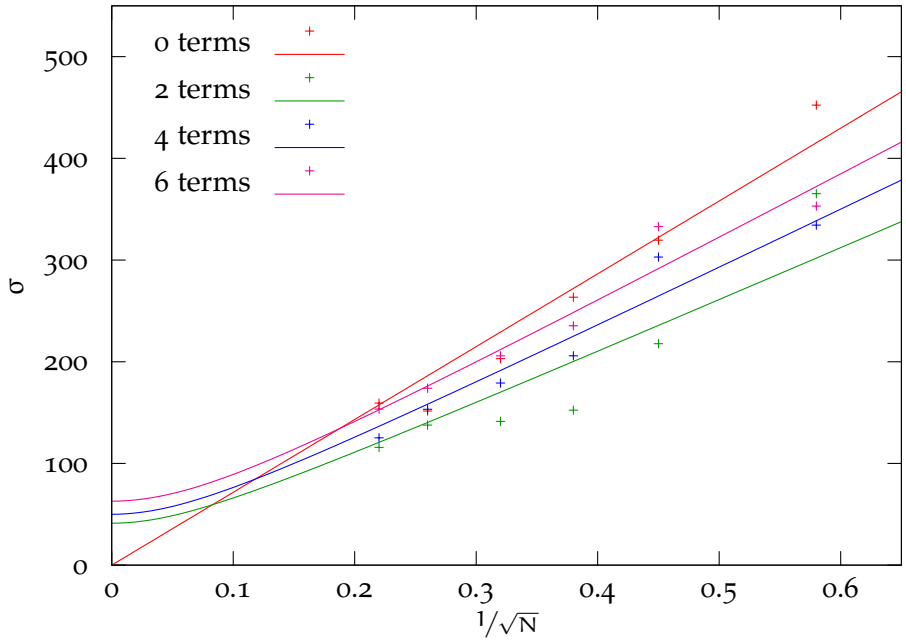

Figure A.9: Standard deviation after 15 seeds for Re $\left[\mathrm{Tr}\left(\mathbb{1} \cdot D^{-1}\right)\right]$ of an E2 configuration calculated with HPE and $M = 200$ sources for the additional terms

The A5 Lattice

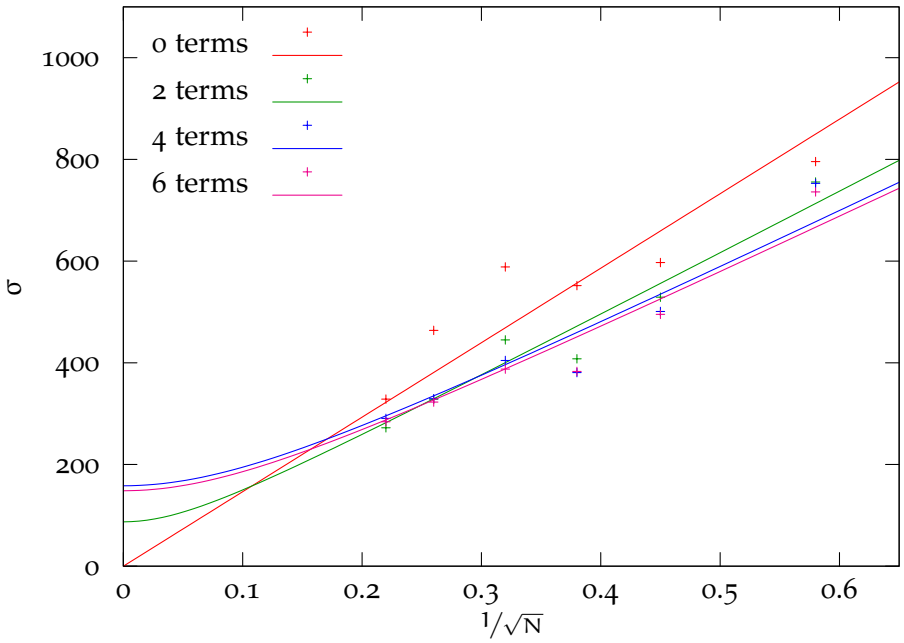

Figure A.10: Standard deviation after 15 seeds for Re $\left[\mathrm{Tr}\left(\mathbb{1}\cdot D^{-1}\right)\right]$ of an A5 configuration calculated with HPE and $M = 50$ sources for the additional terms

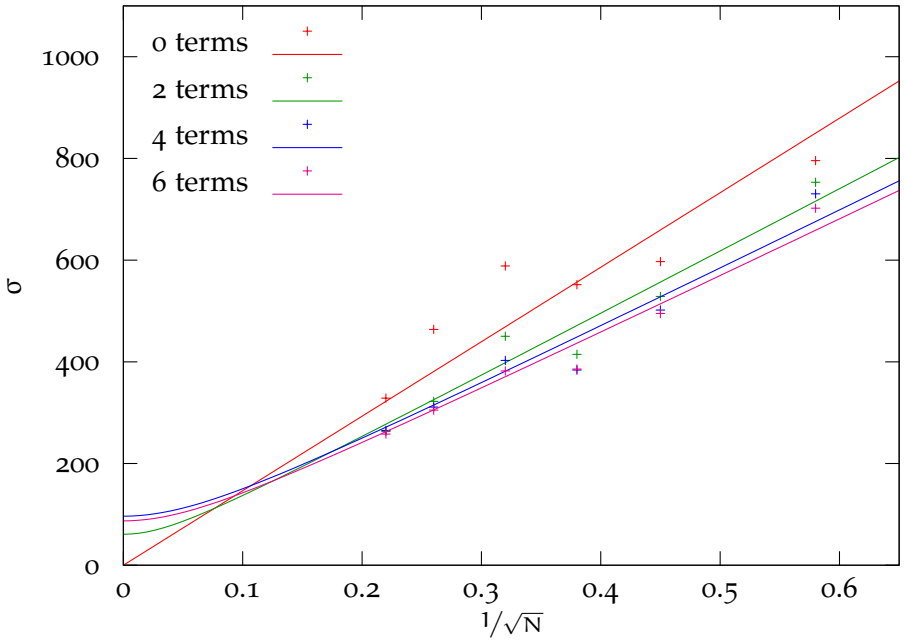

Figure A.11: Standard deviation after 15 seeds for Re $\left[\mathrm{Tr}\left(\mathbb{1}\cdot D^{-1}\right)\right]$ of an A5 configuration calculated with HPE and $M = 100$ sources for the additional terms

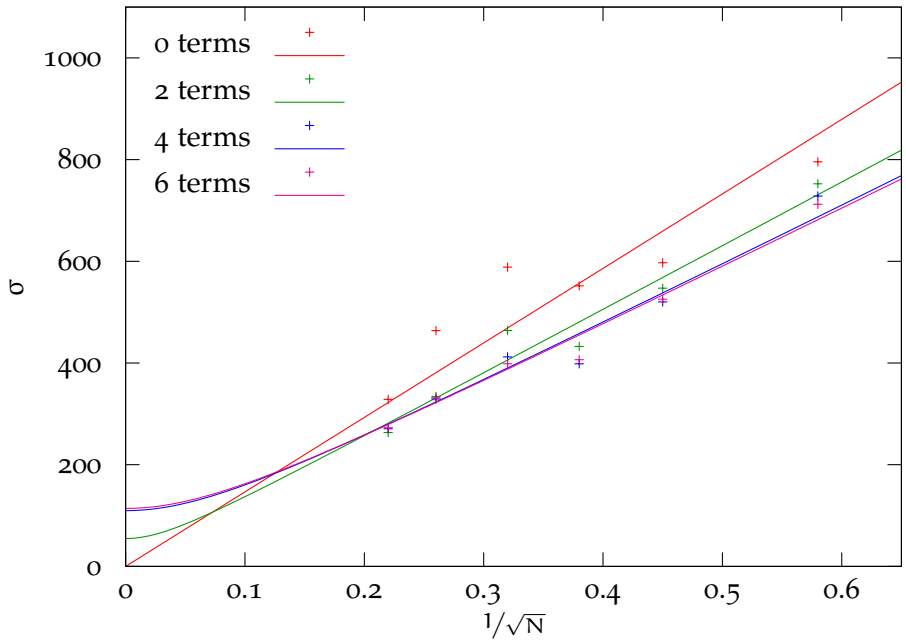

Figure A.12: Standard deviation after 15 seeds for $\mathrm{Re}\left[\mathrm{Tr}\left(\mathbb{1}\cdot D^{-1}\right)\right]$ of an A5 configuration calculated with HPE and $M = 200$ sources for the additional terms

LIST OF FIGURES

BIBLIOGRAPHY

[1] C. Burgess and G. Moore, *The Standard Model – A Primer* (Cambridge University Press, 2007).

[2] M. E. Peskin and D. V. Schröder, *An Introduction to Quantum Field Theory* (Westview Press, 1995).

[3] K. Wilson, "Confinement of quarks," Phys. Rev. D **10**, 2445 (1974).

[4] S. Aoki et al., "Pion form factors from two-flavor lattice QCD with exact chiral symetry," Phys. Rev. D **80**, 034508 (2009), [arXiv:0905.2465].

[5] G. Bali, S. Collins, and A. Schäfer, "Hunting for the strangeness content of the nucleon," PoS **LAT2008**, 161 (2008), [arXiv:0811.0807].

[6] J. F. Donoghue, J. Gasser, and H. Leutwyler, "The decay of a light Higgs boson," Nucl. Phys. B **343**, 341–368 (1990).

[7] T. Draper, R. M. Woloshyn, W. Wilcox, and K. Liu, "The Pion form factor in lattice QCD," Nucl. Phys. B **318**, 319–336 (1989).

[8] K. Bitar and A. D. Kennedy, "The QCD finite Temperature Transition and Hybrid Monte Carlo," Nucl. Phys. B **313**, 348–376 (1989).

[9] G. S. Bali, S. Collins, and A. Schäfer, "Effective noise reduction techniques for disconnected loops in Lattice QCD," Comput. Phys. Commun. **181**, 1570–1483 (2010), [arXiv:0910.3970].

[10] L. Maiani, G. Martinelli, M. L. Paciello, and B. Taglienti, "Scalar Densities and Baryon Mass Differences in Lattice QCD with Wilson Fermions," Nucl. Phys. B **293**, 420–444 (1987).

[11] K. Nakamura et al. (Particle Data Group), "Review of Particle Physics," Journal of Physics G **37** (2010).

[12] J. Goldstone, A. Salam, and S. Weinberg, "Broken symmetries," Phys. Rev. **127**, 965–970 (Aug 1962).

[13] F. Scheck, *Quantum Physics* (Springer, 2007).

[14] S. Capitani, C. Gattringer, and C. B. Lang, "Pion form factor with chirally improved fermions," PoS **LAT2005**, 126 (2005), [arXiv:hep-lat/0509030].

[15] D. Brömmel, *Pion Structure from the Lattice*, Dissertation, Universität Regensburg (2007), URL: http://pubdb.desy.de/fulltext/getfulltext.php?lid=5407&fid=11972.

[16] D. Brömmel et al., "The pion form factor from lattice QCD with two dynamical flavours," Eur. Phys. J. C **51**, 335–345 (2007), [arXiv:hep-lat/0608021].

[17] B. Brandt *et al.*, "Wilson fermions at fine lattice spacings: scale setting, pion form factors and (g-2)$_\mu$," arXiv:1010.2390.

[18] B. Ananthanarayan, I. Caprini, G. Colangelo, J. Gasser, and H. Leutwyler, "Scalar form factors of light mesons," Nuclear Physics B **602**, 218–225 (2004), [arXiv:hep-ph/0409222].

[19] C. Gattringer and C. B. Lang, *Quantum Chromodynamics on the Lattice* (Springer, 2010).

[20] I. Montvay and G. Münster, *Quantum Fields on a Lattice* (Cambridge University Press, 1994).

[21] H. J. Rothe, *Lattice Gauge Theories* (World Scientific, 1997).

[22] J. Smit, *Introduction to Quantum Fields on a Lattice* (Cambridge University Press, 2002).

[23] H. Wittig, "QCD on the lattice," in *Theory and Experiments, Landolt-Börnstein-Group I Elementary Particles, Nuclei and Atoms, Volume A.* (Springer, 2008).

[24] H. B. Nielsen and M. Ninomiya, "A No-Go Theorem for Regularizing Chiral Fermions," Phys. Lett. B **105**, 219 (1981).

[25] L. Susskind, "Lattice fermions," Phys. Rev. D **16**, 3031–3039 (1977).

[26] P. H. Ginsparg and K. Wilson, "A remnant of chiral symmetry on the Lattice," Phys. Rev. D **25**, 2649–2657 (1982).

[27] K. Symanzik, "Continuum limit and improved action in lattice theories," Nucl. Phys. B **226**, 187 (1983).

[28] B. Sheikholeslami and R. Wohlert, "Improved continuum limit lattice action for QCD with wilson fermions," Nucl. Phys. B **259**, 572 (1985).

[29] M. Lüscher, S. Sint, R. Sommer, and P. Weisz, "Chriral symmetry and O(a) improvement in lattice QCD," Nucl. Phys. B **478**, 365–400 (1996), [arXiv:hep-lat/9695938].

[30] M. Lüscher, S. Sint, R. Sommer, P. Weisz, and U. Wolff, "Non-perturbative O(a) improvement of lattice QCD," Nucl. Phys. B **491**, 323–343 (1997), [arXiv:hep-lat/9609035].

[31] M. Lüscher, "Computational Strategies in Lattice QCD," arXiv:1002.4232.

[32] N. Metropolis *et al.*, "Equation of State Calculations by Fast Computing Machines," J. Chem. Phys. **21**, 1087 (1953).

[33] S.J. Dong and K.F. Liu, "Stochastic estimation with Z_2 noise," Phys. Lett. B **328**, 130–136 (1994), [arXiv:hep-lat/9308015].

[34] J. Foley *et al.*, "Practical all-to-all propagators for Lattice QCD," Comput. Phys. Commun. **172**, 145–162 (2005), [arXiv:hep-lat/0505023].

[35] M. Lüscher, "Implementation of the lattice Dirac operator," (2006), unpublished notes.

[36] S. Collins, G. S. Bali, and A. Schäfer, "Disconnected contributions to hadronic structure: a new method for stochastic noise reduction," PoS **LAT2007**, 241 (2007), [arXiv:0709.3217].

[37] W. H. Press, S. A. Teukolsky, W. T. Vetterling, and B. P. Flannery, *Numerical Recipes*, 3rd ed. (Cambridge University Press, 2007).

[38] M. Lüscher, "Schwarz-preconditioned HMC algorithm for two-flavour lattice QCD," Comput. Phys. Commun. **165**, 199–255 (2005), [arXiv:hep-lat/0409106].

[39] M. Lüscher, "Solution of the Dirac equation in lattice QCD using a domain decomposition method," Comput. Phys. Commun. **156**, 209–220 (2004), [arXiv:hep-lat/0310048].

[40] gnuplot(Mai 2011), http://www.gnuplot.info.

[41] G. von Hippel *et al.*, "D_s physics from fine lattices," PoS **LAT2008**, 227 (2008), [arXiv:0810.0214].

[42] B. Jäger, *Lattice Determination of the Leading Order Hadronic Contribution to the anomalous magnetic Moment of the Muon*, Diploma thesis, Universität Mainz (2010), unpublished.

[43] G. von Hippel and B. Jäger, private communication.

[44] E. Endress, A. Jüttner, and H. Wittig, "Stochastic volume sources for the determination of light meson masses on the lattice," In preparation.

[45] S. Capitani, B. Knippschild, M. Della Morte, and H. Wittig, "Systematic errors in extracting nucleon properties from lattice QCD," PoS **LAT2010**, 147 (2010), [arXiv.1011.1358].

[46] M. Della Morte and A. Jüttner, "New ideas for $g-2$ on the lattice," PoS **LAT2009**, 143 (2009), [arXiv:0910.3755].